Design of a Remote Person View System for a Long Range UAV

Pedro de Oliveira Martins Gersão Miller

Thesis to obtain the Master of Science Degree in

Aerospace Engineering

Supervisor: Prof. André Calado Marta

Examination Committee

Chairperson: Prof. Filipe Szolnoky Ramos Pinto Cunha
Supervisor: Prof. André Calado Marta
Member of the Committee: Prof. Agostinho Rui Alves da Fonseca

June 2015

"Be the change you wish to see in the world."

- Mahatma Gandhi

Acknowledgments

I want to dedicate this section to thank my supervisor Professor André Marta for his dedication throughout the elaboration of this dissertation. I would also like thank Professor Agostinho Fonseca for his helpful advice and Professor Carlos Fernandes for kindly providing his useful information upon estimating ranges. I would also like to thank Bernardo Reis for so eloquently flying the UAV and Alexandre Cruz for all his technical support.

This project is the culmination of the last five years of completing my degree which would not be possible without the friends made in this time. So a very special thanks to my classmates who accompanied me throughout the several challenges that arose and without whom this time would not have bee as much fun and fruitful as it was.

I want to express my gratitude to my family for their unconditional and essential support, encouragement and help during all my studies and also during the elaboration of this thesis.

Finally I would like to thank Maria Ana Silva, who makes hard work easier every day.

Resumo

Veículos aéreos não tripulados (UAV) nasceram no sector militar e evoluíram de forma exponencial nos últimos anos devido ao facto de serem vistos como uma abordagem barata e dispensável a missões de alto risco, secretas ou politicamente sensíveis. Estão de facto, a ganhar uma má reputacão mas um número cada vez maior de industrias civis está a tomar proveito desta evolução tecnológica para um bem maior. São uma abordagem viável em detecção e prevenção de fogos, operações de salvamento, agricultura de precisão ou jornalismo.

Nesta dissertação, é abordada e analisada uma solução para pilotagem remota de um destes veículos para aplicações a longas distâncias utilizando equipamento comercial. Para o sucesso desta dissertação foram definidos e explicados objectivos de missão e requisitos para o veículo. O design final é sujeito a testes em ambiente controlado e ensaios em voo e a performance do UAV é, assim, utilizada para avaliar as soluções iniciais e propôr uma configuração final para um veículo aereo não tripulado capaz de percorrer longas distancias sem perder recepção de controlo e transmissão de vídeo.

A plataforma em causa está dividida em três sistemas principais: o controlo remoto, o sistema de vídeo e o rádio de telemetria que, juntos, ligam o UAV à estação de terra. Como forma de avaliar o desempenho do sistema de controlo foi utilizado o parâmetro indicador de força de sinal recebido (RSSI) enquanto que para avaliar o sistema de vídeo foram utilizados parâmetros como perdas por propagação, polarização e obstrução.

Apesar das dificuldades em definir um alcance de voo máximo do sistema global, a solução encontrada provou ter utilidade para aplicações de longo alcance.

Palavras-chave: RPV, UAV, longo alcance, vídeo, controlo remoto

Abstract

Unmanned Air Vehicles (UAV) made their way through the military sector. They have evolved exponentially in the last decade due to the fact that they are seen as a low cost and expendable way for highly dangerous, secret or politically sensitive missions. They are, in fact, getting a bad reputation but a large number of civil applications are taking advantage of these technological advancements for a greater good. Sensor technology, data processing hardware and software algorithms have made the Unmanned Aircraft System (UAS) a highly feasible approach in fire detection, rescue operations, precision agriculture, maintenance or journalism.

A solution for RPV using commercial off-the-shelf (COTS) equipment is presented and analyzed. An Unmanned Air Vehicle (UAV) design was proposed and evaluated through, not only, in a controlled environment but also flight testing. The performance of this UAV was, then, used to evaluate the choices made and purpose a definite and better solution for Long Range Unmanned Air Systems.

The platform in question is a glider and is composed by three main systems: the radio control, the video feed and the telemetry radio that together connect the UAV to the ground station. The parameter received signal strength indicator (RSSI) was used for control evaluation. While propagation, polarization and obstruction losses were used for evaluation of the video system.

Although the long range system encountered difficulties in reaching a maximum flight range, it proved to be useful for long range applications.

x

Contents

List of Tables

List of Figures

List of Acronyms

FHSS   Frequency Hopping Spread Spectrum

GPS   Global Positioning System

LiPo   Lithium Polymer

LOS   Line Of Sight

LRS   Long Range System (radio control)

OSD   On-Screen Display

PPM   Pulse Period Modulation

RC   Radio Control

RPV   Remote-Person View

RSSI   Received Signal Strength Indicator

Rx   Receiver

Tx   Transmitter

UHF   Ultra High Frequencies

UAV   Unmanned Air Vehicle

VHF   Very High Frequencies

List of Symbols

P_r Power available at the input of the receiving antenna

P_t Output power of the transmitting antenna

G_r Gain of the receiving antenna

G_t Gain of the transmitting antenna

λ Wavelength

R Distance between antennas

c Speed of light

f Frequency

F_M Fade Margin

Chapter 1

Introduction

1.1 Motivation

Unmanned Air Vehicles (UAV) made their way through the military sector. They have evolved considerably in the last decade due to the fact that they are seen as a low cost and expendable way for highly dangerous, secret or politically sensitive missions. They are, in fact, getting a bad reputation but a large number of civil applications are taking advantage of these technological advancements for a greater good. Sensor technology, data processing hardware and software algorithms have made the UAV a highly feasible approach in fire detection, rescue operations, precision agriculture, maintenance, journalism coverage and inspection of critical zones [1].

Figure 1.1: UAVs helping farmers [2].

As technology improved and considerably dropped in price, hobbyists and other interested and skilled people have been coming up with all kinds of creative uses for unmanned aerial vehicles. Until now drones have found applications in:

- Farming (Fig.1.1): Farmers have an important but tough job and unmanned air vehicles (UAV) are a great way to do aerial surveys of crops so that farmers can see if their irrigation systems are working, how their plantations are growing or even see if any plantation is affected by pests and diseases by using infra-red sensory [2];

- Sports Coverage: UAVs are a great way of covering a sport event from above; not only is it enter-

taining to watch but it also gives coaches a unique and valuable perspective on how their players are doing [3];

- Law enforcement: Police departments use UAVs for surveillance and related activity and border patrolling [4];

- Environment: All kinds of scientists are using UAVs to keep track of the environment, for example to the United States Environmental Protection Agency (EPA) testing air quality [5]. NASA is using UAVs to probe ozone loss and, in Italy, UAVs have been monitoring on illegal dumping for years [6];

- Wildfire Control (Fig.1.2): UAVs are becoming an incredibly useful tool for fire fighters, especially those who have the seemingly impossible task of putting out wildfires. The aircraft are used not only for spotting and gauging their movement but also actually fight fires, while keeping the fire fighters away from harm [7];

- Transportation: In a situation where a non-profit organisation manages to stockpile medicine for people in remote African villages, but cannot get to the remote areas fast enough to save lives, UAVs can make all the difference. An example is Matternet, a company that is building a network for drone-based deliveries to remote areas [8].

Figure 1.2: UAVs wildfire aiding [7].

1.2 State of the Art

Nyquist [9] describes a project developed by the Oak Ridge National Laboratory that made use of a radio controlled aircraft that was modified to carry a 35 mm video camera and transmitter. The system was designed to collect aerial photography for environmental site characterisation and management, update aerial photos of solid waste storage areas and document construction activities.

Quilter and Anderson, [10] mounted a 35 mm camera in a model aircraft to obtain low altitude/large scale photography to document stream and riparian restoration projects.

In 2002, Stanley Herwitz, professor of Earth Sciences at Clark University, Worcester, was awarded a NASA grant to fund the UAV Coffee Project [11]. The project deployed the UAV Pathfinder-Plus to collect high resolution, multi-spectral imagery to evaluate coffee bean ripeness.

In 2003, Simpson et al. [12] designed a remote person-view (RPV) that featured a modified commercially available model sailplane by installing a Jeti Phasor electric motor, a Opto speed controller and 12-cell, 2400 mAh battery pack. Live video from a single board camera was transmitted from the plane to a ground station and was recorded on VHS video. The sensor platform also included a digital 2 MegaPixel camera with the capacity to store 50 images. The RPV weighed 3.4 kg making it light enough to hand launch and it was able to withstand 'belly landings'. The simplicity of the plane allowed for easy transport and on-site data review.

The platform used by Hardin and Jackson [13] in 2005, was designed to include remotely controlled aircraft with a flight stabiliser, a 35 mm camera and a GPS receiver. Upon landing, the GPS data was downloaded, yielding the plane's vertical and horizontal positions and velocity. The photograph locations were found by following the GPS tracks.

As part of the Global Dust Program, the United States Geological Survey (USGS) designed a UAV to identify micro-organisms that can survive long-range atmospheric transportation by desert dust clouds. The study used a one-quarter scale Super Cub aircraft with a wingspan of 2.5 m and nitro-engine combination capable of carrying 14 kg for one hour duration at an altitude of one kilometre [14]. The UAV telemetry included real-time positioning, autonomous scientific instrumentation control, autonomous flight and ground control and a lightweight precision vision system.

In [15] a modified radio control (RC) aircraft equipped with a GPS receiver and a digital camera was proposed to conjunction with automated post-processing techniques to reduce the costs of traditional noxious weed mapping. The study found that the automated post-processed photos were not positioned sufficiently accurate to produce consistent and accurate weed perimeters. In order to increase the accuracy of the weed maps, the project had to rectify the photos and hand digitized the weed perimeter which was time intensive and the associated costs exceeded the traditional on foot method.

The Virginia Polytechnic Institute and State University integrated MicroPilot technology for precise aero-biological sampling above agricultural fields. Five different flight patterns were explored to determine the most appropriate sampling path for aero-biological sampling above crop. The project completed 25 sampling flight tests, conducted from 10 m to 100 m above agricultural fields. The study concluded that an orbital sampling pattern around a single GPS waypoint exhibited high positional accuracy with altitude standard deviations [16].

In 2012, Roberto Montiel broke the world record for range in a remote control model glider using a camera onboard. Most of the flight was done soaring power off, taking advantage of thermal air updrafts. The starting point was Algora, Spain and the route extended SouthEast 111 km and return to the start, 222 km. The total flight time was 6 hours.

1.3 Project Framing

The present dissertation is part of the project of a long endurance electric unmanned aircraft vehicle which is being developed in a collaborative project by the departments IDMEC (from Instituto Superior Técnico), INEGI (Faculdade de Engenharia da Universidade do Porto) and AeroG (Universidade

da Beira Interior) under the sponsorship of LAETA (Laboratório Associado de Energia, Transportes e Aeronáutica) [17].

The main goal of the project is to develop a low cost, smart footprint electric UAV, capable of being deployed from short airfields, easy to build and maintain, and high flexible to perform different civilian surveillance missions. The main specifications of the RPV system include:

- Long Endurance: accomplished by using green power technologies such as an electric propulsion system with solar power. This includes the use of highly efficiency solar cells, high capacity/density batteries, efficient compact motors and appropriate long endurance aerodynamic design;

- Autonomous Flight: accomplished by equipping the UAV with autopilot navigation systems such as inertial guidance systems and GPS;

- Obstacle Avoidance: accomplished by implementing an obstacle avoidance technique that includes detection, estimation, and avoidance planning of the obstacle;

- High-Strength, Low-weight Structure: accomplished by using composite materials, with fuselage/wing critical areas designed for good impact resistance on landing, using easy to manufacture techniques;

- Multiple Mission: accomplished by designing a sufficiently large payload range capability and developing upgradable modular avionics, to enable easy software upload and/or hardware swap to meet the selected mission requirements.

For the elaboration of these requirements and specifications of the RPV system, a plan was made with the following tasks:

1. Conceptual Design - At this stage, several configurations are evaluated where the goal is to meet or exceed the mission requirements: endurance, size and cost;

2. Propulsion System - Secondly, several electric propulsion system configurations are considered, comparing electric performance, weight and cost. Solar panels are selected in function of the electric brushless motors;

3. Aerodynamic Design - Definition of the wing geometry. Wing is sized for the propulsion system, avionics and auxiliary systems; Tail is designed from first considerations of static stability. As the design progresses, their geometry will most likely have to be revisited;

4. Noise Prediction - Here, the mechanisms associated with wing and airframe noise generation will be addressed. Analytical codes will be implemented for the UAV in study, that will be taken as input variables for the optimisation study;

5. Structural Design and Aeroelastic Analysis - The airframe both internal structures and external skins is designed in this task with the goal of achieving a light and strong enough structure, while keeping its manufacturing cost reasonable;

6. Design for Manufacturing - manufacturing feasibility and integration study is undertaken in order to ensure the manufacturability of the proposed designs;

7. Stability and Control - During this task, the control surfaces are designed to provide enough stability and control authority to the aircraft. Empirical data is used and the results are tuned in wind tunnel testing. The data gathered from wind tunnel testing is used to develop the UAV controller;

8. Multidisciplinary Design Optimisation - At this point, all the necessary analysis tools for the propulsion, aerodynamics, structures and controls are in place. As such, it is possible to couple all these into a multidisciplinary optimisation framework to refine the aircraft design;

9. Communication and Electronics - In this task, the communications and electronic systems are established. There are several goals for this task: design and implement the autopilot hardware and software, make the aircraft systems capable of flight logging and possibly telemetry to a ground station, and install all the sensors and actuators in the airframe. Aerothermodynamic analysis is performed with the aim of managing the thermal loads from the internal avionics to guarantee efficient cooling in the expected tight bay. Telemetry equipment is installed to monitor the aeroelasticity behaviour;

10. Manufacturing - Here, the construction of the UAV is accomplished. The goal is to build the airframe according to the detailed structural design, using advanced model building techniques. A total of two models is built, a first generation prototype and a second generation prototype;

11. Flight Testing - The full-scale prototypes testing includes systems checks on ground, wind tunnel tests to assess aerodynamic performance, static thrust under varying solar conditions and, finally, flight tests. The first aircraft is operated under radio controlled mode, which allows for through checks of the solar powered propulsion system. The second aircraft is used to test the overall design refinement and also the autopilot hardware and software.

As for this dissertation, its focus falls into the Communications and Electronics task where its objective is to implement both a video and radio control systems capable of responding the long endurance requisites of the project. The mission profile for the LAETA project can be summarised as follows:

1. Take-off at sea level with mass 4.9 kg;

2. Climb up to 1000 m altitude;

3. Fly for 8 hours in the equinox (21 March or 21 September) at an altitude of 1000 m at low speed to be defined by system efficiency but greater than 6 m/s and maximum speed of 21.1 m/s;

4. Descent;

5. Landing in the field at sea level.

1.4   Objectives

The objectives of this thesis are design, construct and test a remote-person view (RPV) system, in order to control a long endurance electric UAV. The expected results include detailed design, setup and test

of the control and video subsystems for the unmanned air system (UAS) of a long endurance electric UAV. The tests will be done in a way that both video and remote control are approved in a controlled environment and then perform a series of flight tests where both systems are evaluated in its range and quality.

1.5   Structure of the Document

This work is divided in four main stages: the design of the control and video sub-systems (Chapters 3 and 4), setup of the whole Unmanned Air System (Chapter 5), testing in controlled environment (Chapter 6), flight testing and conclusions (Chapters 7 and 8).

In Chapters 2, 3 and 4 it is made a description of typical RPV systems, including both control and video sub-systems followed by a benchmark of commercial solutions. Then comes a detailed description of the design of both the control and video sub-systems and construction of the same (Chapter 5).

After characterizing the whole unmanned air system, both control and video sub-systems are tested in a controlled environment (Chapter 6) followed by flight testing (Chapter 7) and the respective results are presented.

Chapter 2

Description of the RPV System

2.1   Description of UAV Systems

An unmanned aerial vehicle is an airborne vehicle without a human crew on-board. Historically, the term and the primary use of UAVs have been in the military area. Continuous development and technology transfer has lowered the cost of accessing the technology outside the military domain. This has allowed for expanding the use of unmanned aerial vehicles to many civilian applications.

In recent years, the term UAV has been replaced with the term UA which stands for unmanned aircraft. To emphasize that a UA is a part of a complete system including ground operator stations, launching mechanisms and so forth, the term unmanned aerial system (UAS) has been introduced and its use is becoming commonplace [18].

One common feature of UASs is the use of a video system. This system allows the UAV to be piloted beyond the line of sight of the pilot from a first-person perspective via an on-board camera fed wireless to a monitor.

In order to describe the components that constitute the desired UAS for this dissertation, the platform was divided into two sub-systems, as seen in Fig. 2.1: the airborne and ground station setup and the means of communication between the two.

In the chapters that follow, the UAS was divided between video and control systems instead of the airborn and ground station systems.

The following subsections aim to give an overall view of these sub-systems.

2.1.1   Airborne

The airborne equipment refers to the systems that will be flying. The type and performance of the aircraft is determined by the needs of the operational mission. For horizontal take-off and landing (HTOL) aircraft the flight variables are direction, horizontal speed, altitude and rate of climb. The direction of flight (heading) will be controlled by a combination of the servos responsible for the rudder and ailerons; the horizontal speed will be controlled by voltage regulator of the propulsive thrust and elevator deflection. Finally, the rate of climb to a given altitude is achieved by the application of a combination of elevator
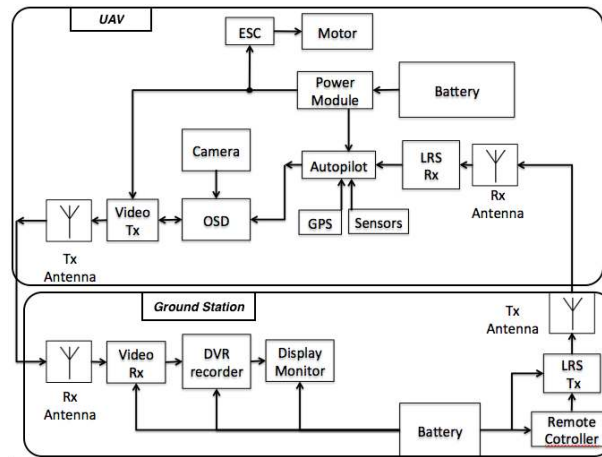
Figure 2.1: UAS - Functional structure.

deflection and propulsive thrust. All the servos are connected to the receptor that receives orders from the transmitter (or autopilot depending on the type of flight operation).

As for the navigation system described below, the degree of autonomy in a UAS can vary greatly, ranging from teleoperation to fully autonomous operation. Teleoperation is a mode of operation where the UAV is commanded by a human operator using a remote controller from the ground. In this mode of operation, the degree of autonomy is minimal because continuous input from an operator is required. Fully autonomous UAVs are characterized by the ability to maintain flight and to carry out complete missions from take-off to landing without any human pilot intervention.

Regarding ways of navigation, the operator can be either piloting the UAV from sight which gives the system a reduce area of operation or it can be piloted through a video system monitor which gives the pilot an on-board view. This type of piloting is usually called remote person view (RPV) and greatly increases the usable operating area of the UAV. For this, telemetry readings and a video transmission will take part of the onboard equipment. This way, an example of an airborne system is shown in Table 2.1 and Fig. 2.2.

Equipment	Description
Actuators	Small, mass-produced servomotors used for radio control.
Engine and propeller	Machine designed to convert one form of energy into mechanical energy.
Battery	Converts stored chemical energy into electrical energy
Video Transmitter (Tx)	Transmits audio and/or video signals wireless from one location to another
Video Camera	Captures video that, in this case, becomes the eyes of the pilot.
RC receiver (Rx)	Receives radio control signals from a source and processes them to the actuators
Flight Controller	allows the operator to turn any vehicle into fully autonomous capable of performing programmed GPS missions with waypoints
Transmitting Antenna	Radiates the energy from the transmitter as electromagnetic waves
Receiving Antenna	intercepts some of the power of an electromagnetic wave in order to produce a voltage at its terminals that is applied to a receiver to be amplified and interpreted.

Table 2.1: Airborne equipment necessary for RPV operations.
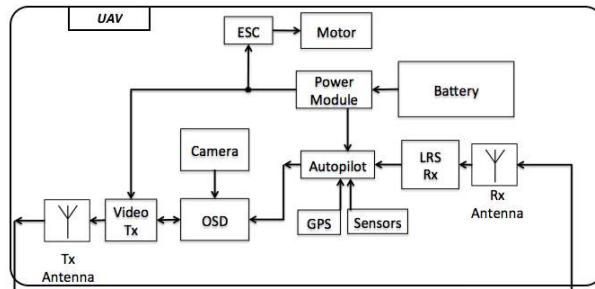
Figure 2.2: Airborne equipment necessary for RPV operations.

2.1.2 Ground Station

The control station is based on the ground and it is the control centre of the operation and the man-machine interface. It is, usually, the platform in which the mission is pre-planned. In a similar way, via the communications down-link, the aircraft returns information and images to the ground station operators. This information may include data from the payloads, status information of the sub-systems and position information. This way, an example of a ground station is shown in Table 2.2 and Fig. 2.3:

Equipment	Description
Battery	Converts stored chemical energy into electrical energy;
Video Receiver (Rx)	Receives audio and video signals from a number of sources and process them to drive loudspeakers and a display;
Video Recorder (DVR)	Records video in a digital format to a memory storage unit;
Radio Control Transmitter (Tx)	Generates a radio frequency alternating current which is applied to the antenna. When excited by this alternating current, the antenna radiates radio waves;
Display Monitor	Electronic visual display for video system;
Transmitting Antenna	Radiates the energy from the transmitter as electromagnetic waves
Receiving Antenna	Intercepts some of the power of an electromagnetic wave in order to produce a voltage at its terminals that is applied to a receiver to be amplified and interpreted.

Table 2.2: Ground station equipment necessary for RPV operations.
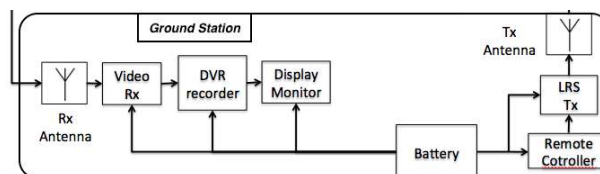
Figure 2.3: Ground station equipment necessary for RPV operations.

The launch equipment can take the form of a ramp along which the aircraft is accelerate on a trolley, until the aircraft reaches an airspeed at which it can sustain airborne flight. On the other hand, the recovery equipment is usually a parachute or even a set of wheel that allow the aircraft to land in a run-on landing. For the particular case of RPV system used in this work, it will be hand launched and prepared for belly landing.

For simplification, in this thesis the systems are divided into control (that goes airborne and in the ground) and video (that goes airborne and in the ground).

2.2 Legislation

2.2.1 Bandwidth Legislation

The authority that regulates radio frequencies in Portugal is ANACOM (Autoridade Nacional de Comunicações). There is a document publicly available [19] that defines the bandwidth of frequencies available for amateur radio control and video transmissions. Table 2.3 was built from that data.

Bandwidth [MHz]	Applications
430-440	Amateurs and Local Radio
1240-1300	Amateurs
1260-1270	Amateurs
2300-2400	Amateurs and Local Radio
5650-5670	Amateurs
5668-5670	Amateurs
5670 - 5725	Amateurs
5725 - 5830	Amateurs
5830 - 5850	Amateurs and Local Radio

Table 2.3: Attribution of frequencies by ANACOM.

Summarizing, with the respective license, there is the possibility of choosing the frequencies in Table 2.3 for applying in this dissertation. This will later be taken into account when selecting the components used for the designed RPV system.

2.2.2 UAV Flying Legislation

A quick research in local newspapers lead to the conclusion that the Portuguese government is yet to build a clear law on UAVs. However, in later months, that empty space has been reduced by the *Instituto Nacional de Aviação Civil* (INAC) by proposing a law in that sense. The use of any UAV would depend on the authorization of INAC, limiting its access to the segregated aerial space so that UAVs are not used in/near the normalized aerial traffic.This discussion on the regulation of UAV flights was first presented in [20].

2.3 RPV System Requirements

The airframe and components chosen will have to take in consideration a set of requirements. Some of the requirements can be derived from Section 1.3:

- The weight of the vehicle must be as low as possible to allow an efficient flight and small vehicle size and to allow operation in very small airfields. Also, it should be able to carry a payload up to 1 kg;

- The airspeed in the cruise/loiter phase of 8 hours should be about 7 m/s (25 km/h), at an altitude of 1000 m;

- Develop a low cost, small footprint electric UAV.

The range of the RPV system must correspond to the 8 hours of flight, meaning that at a speed of 25 km/h with 4 hours for going and 4 more to come back the maximum distance between the ground station and the aircraft will be 100 km. Figure 2.4 represents an idea of the coverage that the UAS could provide in national territory.
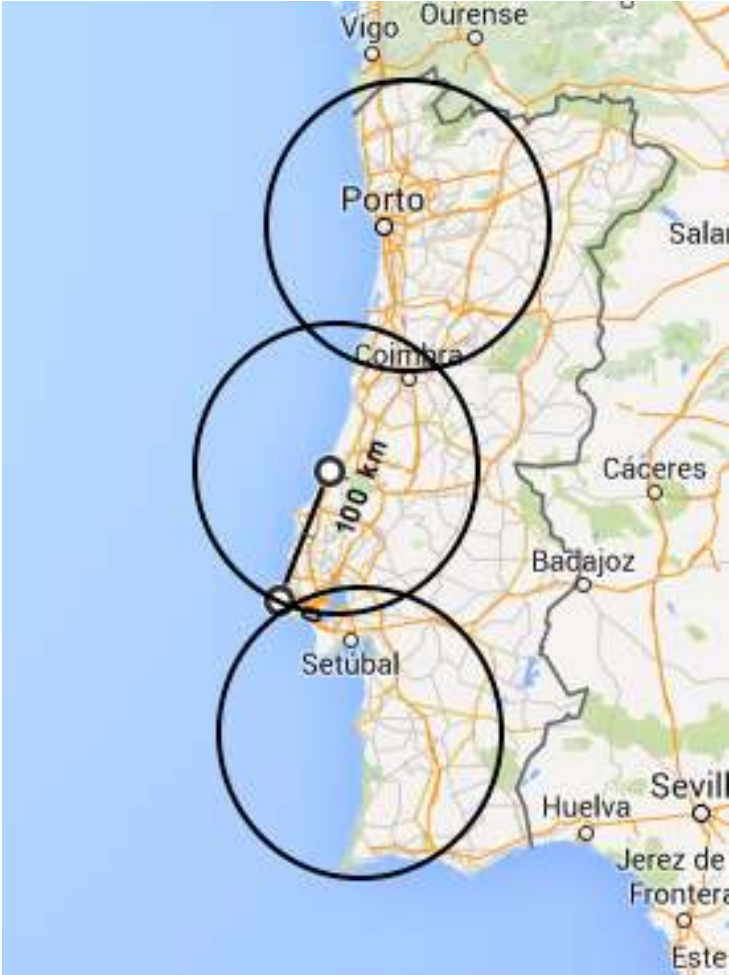
Figure 2.4: UAS coverage assuming a 100 km range along the portuguese coast.

Chapter 3

Design of Control System

This chapter aims to describe the design of the control sub-system used for this dissertation in which Commercial-off-the-shelf (COTS) products are used; this includes the primary components such as remote control transmitter, long-range radio receiver and high gain antennas.

Radio control (RC) is the use of radio signals to remotely control a device. The term is used frequently to refer to the control of model vehicles from a hand-held radio transmitter. RC electronics have three essential elements: 1) The transmitter is the controller that has control sticks, triggers, switches and dials at the pilot's finger tips; 2) The receiver that is mounted in the model receives and processes the signal from the transmitter translating it into signals that are sent to the servos; 3) The servos that are mechanical actuators that follow the commands sent by the transmitter and converted by the receiver. In order to perform long endurance flights, two add-ons need to be considered.

- Flight Controller/autopilot;

- Long Range System (LRS).

While the former provides navigation and flight aids, the latter extends the radio control range.

A block diagram of the entire RC unit is presented in Fig. 3.1.
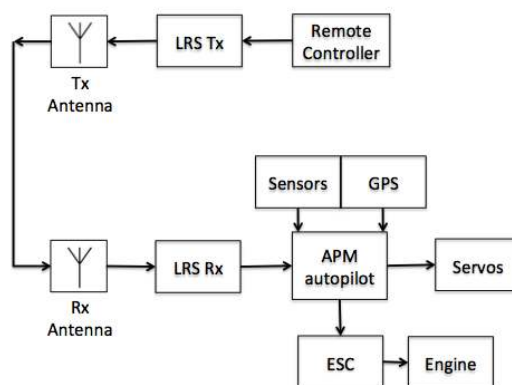
Figure 3.1: Block diagram showing the radio control (RC) sub-system.

3.1 Radio Control System

For radio control, there are three forms of radio frequency (RF) communication systems: 1) simplex (radio technology that allows only one-way communication from a transmitter to a receiver); 2) half-duplex (operation mode in which each end can transmit and receive, not simultaneously); 3) full-duplex (each end can transmit and receive simultaneously). In order to control the UAV from the ground station, a simplex communication system is required. A basic simplex communication system is composed by the building blocks from Fig. 3.2 [21].
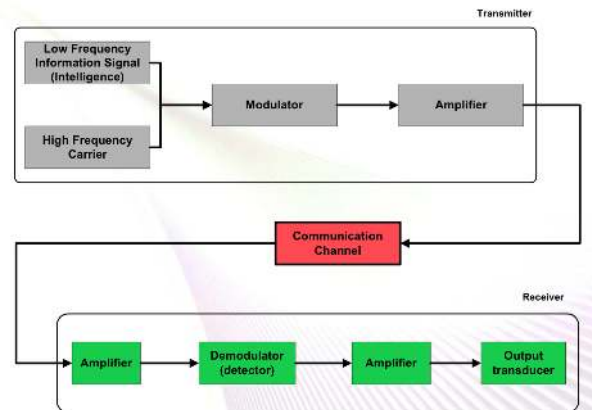
Figure 3.2: Basic building blocks of a RF system.[21].

The RF modulation is part of the transmitter will combine data into a carrier wave at a standardized frequency as required by the receiving equipment. The demodulator, on the other hand, is part of the receiver and will perform analogue demodulation extracting the original information-bearing signal from the modulated carrier wave [21].

The signal output from a demodulator may represent sound (an analogue audio signal), images (an analogue video signal) or binary data (a digital signal).

There are three major types of signal modulation: 1) Pulse-position modulation (PPM) is one form of signal modulation in which message bits are encoded by transmitting a single pulse in one possible time-shift, repeated every t seconds; 2) Pulse-Width Modulation is a technique used to encode a message in a pulsing signal where the average value of voltage (and current) is controlled by turning the switch between supply. It used to relay data in the form of a varying pulse width. The way data is relayed to a servo, for instance, is the time the pulse is on; 3) Frequency Shift Keying (FSK) is a frequency modulation scheme in which digital information is transmitted through discrete frequency changes of a carrier wave [21].

It is desired that the UAV is built out of commercial-off-the-shelf (COTS) solutions and the market offers a variety of radio-link options in a wide spectrum of frequency bands. Manufacturers, usually, provide a whole set of parameters for their links such as:

- **Transmitting Frequency**: The usable frequency spectrum extends from 3 Hz to 300 GHz which is split into standardized regions. As frequency increases, the signal is prone to be absorbed by physical objects (atmospheric moisture, trees, buildings, etc.), hence the need for more power to

make up for signal loss. For constant power, the range decreases with the increase in frequency due to the increase in signal loss. This energy transfer to physical objects is similar to the one behind microwave ovens (which operate in 2.45 GHz) that transfer the transmitted energy to water molecules [22]. Another factor affecting terrestrial communication range is the tendency of low frequencies to follow the curvature of the earth's surface by reflecting off of the atmospheric layers or refracting through atmospheric layer boundaries. This allows the conclusion that the lower the frequency, the longer the communication distance. As frequencies get higher, the tendency is for the signal to pass through the layer boundaries rather than reflecting on them. The result is shorter range with power not being a factor. However, higher frequencies (in the range of GHz) signals have the ability to send signals with much better quality. The aim is to get a system that has a good compromise between signal fidelity and signal quality.

- **Effective Radiated Power (ERP) of the Transmitter**: Effective Radiated Power is the standardized theoretical measurement of radio frequency energy and is determined by subtracting system losses and adding system gains. It takes into consideration transmitter power output, transmission line attenuation (electrical resistance and RF radiation), RF connector insertion losses and antenna gain.

- **Sensitivity of the Receiver**: The sensitivity is a measure of the quality of a receiver and is related to the signal-noise ratio (SNR). Sensitivity is the mnimum magnitude of input signal required to produce a specified output signal [23].

3.1.1 Remote Control Transmitter

The transmitter (Tx) is usually built into the hand-held controller which encodes movement from the fingers of the pilot into several channels of flight control data. Each channel is encoded as a scalar value based on the position of the interface which is usually composed of two joysticks each with two degrees of freedom.

The functionalities to look for in a remote control transmitter are:

- Price;

- Number of channels;

- Modes;

- Compatibility with Long range systems.

Each channel allows one individual function on the aircraft. For example, for turning left or right, for pitching forward or backwards, for throttle and for rolling left or right. Four channels is the minimum for the required UAV (pitch, roll, throttle and yaw).

With a remote with more than four channels, there is the choice of using switches or potentiometers to change settings on the UAV during flight. When using a flight controller the minimum number of channels increases to five, the extra channels is to switch between different flying modes.

Regarding compatibility, the transmitter has to enable PPM signal modulation. In the features of the RC remote there has to be the capability of student function (see list of acronyms) and to be compatible with PC simulators. Its down side is the price being the most expensive component in the whole system with a cost of 1000. €

The Graupner mc-24 was chosen because of it popularity amongst pilots and for its 12 controllable channels (switches and potentiometers) with internal or external telemetry. Also, it gives the pilot the freedom to programme everything like he wants to have it. This becomes helpful when features besides the usual four-servos configuration are added for example when using a camera gimbal onboard or when having an autopilot that has more than one flight mode. Its most important features are: 1) six free configurable flying phases with pre configurable rudder positions and variable switching time; 2) Up to 16 full free configurable switches; 3) Up to eight full free configurable control switches; 3) Trim travel reduction; 4) Servo speed configurable for every servo or control; 5) six programmable clocks; 6) Can be used as teacher/student transmitter; 7) It has four modulation systems: SPCM 20 (10 channels), PCM 20 (10 channels), PPM18 (9 channels), PPM24 (12 channels).

All the mentioned features will allow a more complex UAS where functions that were not thought at the beginning and start to appear as the project grows. For these reasons, the Graupner mc-24 remote controller was selected.

3.1.2   Receiver

The receiver (Rx) interprets the signals from the transmitter and sends them out ot the servos. The receiver must match the transmitter to work properly. They must, be both of the same type, band and channel settings. Most receivers operate at 4.8 V or 6 V. Some have a battery eliminator circuit allowing the connection of a 7.2 or 8.4 V a main battery on an electric model into the receiver. The standard voltage in use is 6 V (equal to a four-cell alkaline holder) and since any of the receiver's channels will accept power input, a full 6 V can be sent to these receivers by connecting the battery to an unused channel or by using a 'Y' harness to connect it to a channel in use by a servo.

3.1.3   Long-Range System (LRS)

A useful COTS upgrade for the RC system for this particular case is an Long Range System (LRS). Typically, they consist of a small box transmitter mounted on the back of the existing transmitter coupled with a matching receiver, like any other that is attached to the on board equipment. The advantage of the LRS is it just connects right to an existing transmitter allowing the RPV model to travel long distances.

The major problem of this system is it might cause electrical interference in the video and disturb it. This happens due to spurious emissions, which refers to any signal that comes out of a transmitter other than the wanted signal. Harmonics is one type of spurious emissions and they are the multiples of the operating frequency of the transmitter. If one harmonic falls on the frequency being used by the video system, then this spurious emission can prevent the video signal from being properly received. To avoid interferences with the harmonics, in addition to the good design of the amplifier, the transmitter output

could be filtered with a low pass filter to reduce the level of the harmonics. The filter will pass the desired frequency and reduce all harmonics to acceptable levels.

Although a lower frequency (like 35 MHz) would provide, theoretically, a longer range, all LRS systems are sold for 433 MHz. This because the law does not allow enough bandwidth per channel to encode digital data and also because high enough emitted output power is not legal [24].

In the following paragraphs, it will be presented a market study on different long range systems that could be implemented. There are many options to choose from and these LRSs were considered because of their popularity within the community. This means there are many reviews and experiments ([25, 26] are just a couple of examples) about them which facilitates the selection process. In order to choose a proper long range system it is important to retain the following requirements:

- Phase Noise of the Transmitter;

- Effective Radiated Power of the Transmitter;

- Sensitivity of the Receiver;

- Estimated Range;

- Price.

Based on the requirements itemized above, four systems are compared for radio control and, in the end, the one with better price/quality ratio is chosen. The systems chosen based on popularity are: the DragonLink, the EZUHF, the OpenLRS and The ThomasScherrerLRS. First, the systems were compared on the harmonics that are represented in Table 3.1.

		Scherrer[25]	EZUHF[25]	DragonLink[25]	OpenLRS[26]
Binded	Frequency [MHz]	433	433	433	433
	Output Power[dBm]	27	27	27	27
3rd Harmonic	Frequency[MHz]	1296	1296	1296	1296
	Phase Noise[dBm]	-64	-48	-50	-80

Table 3.1: Comparison of phase noise and output power of long range transmitters.

With a resonance noise floor of -90 dBm, it is easily noticeable that the OpenLRS has the best transmitter's input filter, meaning that it will be producing much less noise onto a video receiver than the others, being the second best the ScherrerLRS. However, this issue does not mean that the OpenLRS will fly longer ranges, it means that the control and video systems will not interfere with one another as much [26].

The output power of the Scherrer is variable from 0.5 to 2 W; the EZUHF from 0.2 to 0.6 W; the DragonLink from 0.25 to 0.5 W; the OpenLRS has a fixed output power of 1 W.

The physical specifications of the systems are also important as the UAV demands less space, payload and power consumption and they are compared in Table 3.2.

The Scherrer RC system was selected because it has been proved to perform more than 100 km range, Roberto Montiel from Section 1.2, compared with the other systems it is the second with less phase noise.The sensitivity of the OpenLRS is the lowest of the lot. From the type of modulations, all

	Scherrer	Immersion EzUHf	DragonLink	OpenLRS
Size [mm]	26x54x18	70x30x17	49x84x28	N/A
Weight [g]	20	22	22	N/A
Range [km]	100	70	50	N/A
Sensitivity [dB]	-114	-112	-115	-118
Modulation	PPM	FSK	N/A	FSK
LRS Price [€]	450	350	225	160

Table 3.2: Comparison of physical specifications for the long range system.

systems are digital meaning they are less affected by interferences. Analogue signals are constantly changing electromagnetic waves which can be influenced by external electromagnetic fields. Digital signals are electrostatic pulses of a fixed amplitude. They resist external fields because the pulses are either fully on or fully off [22].

This LRS has been used since 2008 in the most diverse applications with proven results. The Tx unit, shown in Fig. 3.3(a), samples PPM frames from a standard remote control Tx unit (from 4 to 12 servo channels) and encodes this data digitally.

(a) Scherrer Tx700.

(b) Scherrer Rx700.
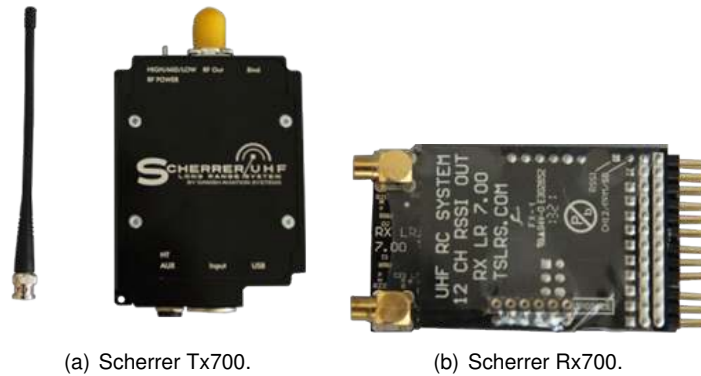
Figure 3.3: Thomas Scherrer long range RC system [27].

The Rx unit, shown in Fig. 3.3(b), decodes the data and generates the desired (up to) 12 pulses, giving a jitter free system known from all pulse code modulation (PCM) systems. At the same time, this system uses a multi frequency hopping (FHSS) making it more immune to jamming. The diversity system, which is choosing the best receiving antenna from having two connected, on the Rx removes blind spots when the angle from the plane to the ground station changes from, for example, a banking manoeuvre if one of the antennas is placed horizontally and the second vertically.

It operates through the UHF band (433 MHz to 440 MHz), has a maximum radiated power of 2 W and has a Receiver Signal Strength Indication (RSSI) analogue output pin that proves to be extremely useful to check during flight.

3.2 Flight Controller

Flight Controller systems are now widely used in modern aircraft and ships. The objective of UAV autopilot systems is to consistently guide UAVs to follow reference paths or navigate through pre-set

waypoints. A powerful UAV autopilot system can guide UAVs in all stages of autonomous flight including take-off, ascent, descent, trajectory following, and landing.

An autopilot also needs to communicate with the ground station for control mode switch, to receive broadcasts from GPS satellites for position updates and to send out control commands to the servo motors on UAV.

A UAV autopilot system is a closed-loop control system with two fundamental functions: state estimation and control signal generation based on the reference paths and the current states. The most common state observer is the Inertial Measurement Unit (IMU) including gyros, accelerometers and magnetic sensors. There are also other attitude determination devices available like infra-red or vision-based ones [28]. The sensor readings combined with the GPS information can be passed to a filter to generate the estimates of the current states for later control uses. Based on different control strategies, the UAV autopilots can be categorized as proportional-integral-derivative (PID)-based autopilots, fuzzy-based autopilots, neutral network (NN)-based autopilots, etc. [29].

A typical commercial off-the-shelf UAV autopilot system comprises of a GPS receiver, an IMU and an onboard processor (state estimator and flight controller) as ilustrated in Fig. 3.4 [28].
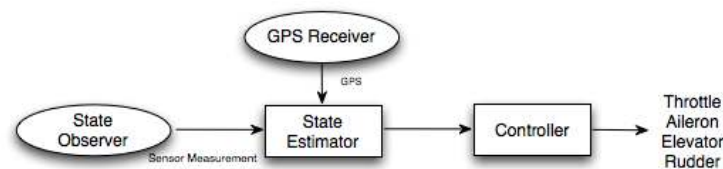
Figure 3.4: Functional structure of the UAV autopilot. [30]

All inertial measurements from sensors are sent to the onboard processor for further filtering and control processing. The strength of the autopilot software directly affects the robustness of the whole autopilot system [29].

There are three basic controllers for the UAV flight control: altitude controller, velocity and heading controller. Altitude controller is to drive the UAV to fly at a desired altitude including the landing and take-off stages. The heading and velocity controller is to guide the UAV to fly through the desired waypoints. To achieve the above control requirements, different control strategies can be used including PID, adaptive neural network, fuzzy logic, and fractional order control. Given the reference waypoint coordinates and the current UAV state estimates, the controller parameters of different layers can be tuned off-line first and re-tuned during the flight. Most commercial autopilots use traditional PID controllers because they are easy to implement in the small UAV platforms. However, PID controllers have limitations in optimality and robustness [28].

For the present work, it is important that the selected autopilot respects the following requirements:

- Small dimensions and weight;

- Low price;

- Waypoint following capabilities;

- Configurable.

The physical specifications of the autopilots are particularly important in small UAVs in which space, payload and power are very limited. Size, weight specifications are shown in Table 3.3.The following flight controllers were chosen due to the relative popularity amongst users: the APM 2.6, the Pixhawk and the RVOSD, the functional specifications are listed in detail in Table 3.4.

	APM2.6	Pixhawk	RVOSD
Size [mm]	67x41x15	5x15.5x81.5	66x40x20
Weight [g]	33	38	32
Price [EUR]	240	280	300
DC In [V]	5 -6	4.1 -5.7	6 -25
CPU [MHz]	168	168	NA
Memory [Mb]	4	4	NA

Table 3.3: Comparison of physical specifications of autopilots [31, 32, 33].

	APM2.6	Pixhawk	RVOSD
Waypoints Navigation	✓	✓	✓
Auto take-off and landing	✓	✓	✓
Altitude Hold	✓	✓	✓
Airspeed Hold	✓	✓	✓
OSD	x	x	✓
Telemetry	x	x	✓

Table 3.4: Comparison of autopilot functions [31, 32, 33].

Regarding the RVOSD and Telemetry functions, its construction means that it is not necessary the acquisition of an On-screen display (OSD), as it is in the case of the other two autopilots, since both functions are already embedded in the system. The APM was chosen because it is the cheapest one of the three, it has been used by many pilots meaning it has proved capabilities and [29] explores its many capabilities.

3.3 Telemetry Radio

The telemetry radio which is a supplement to the APM autopilot, was acquired because it provides an air-to ground data link between the autopilot and the ground station computer. It works as it is a replacement for the USB connection to the computer. This radio, shown in Fig. 3.5 will allow real-time data from the UAV. Since it produces 100 mW minimum of output power it can be said that it is a quiet equipment to the on board receivers. Its drawback is a rather limited range of 2 km. A 3.7 to 6 V voltage range allows a direct connection to the UAV not requiring a voltage regulator. Its main specifications are summarized in Table 3.5.

3.4 Radio Control Antennas

Any radio transmission occurs at a certain frequency, depending on the propagation of speed waves through the air. The geometry of the antenna is based on taking advantage of resonances so that their

Figure 3.5: Telemetry Radio from 3DR Robotics.

Table 3.5: General specifications of 3DR-telemetry radio.

3DR-Telemetry radio	
Frequency	433 MHz
output Power	100 mW
receiver sensitivity	-117 dBm
Communication	Full-Duplex
Protocol Framing	MAVLink
FHSS	
Open-source firmware	
Configurable	
Receive Current	25 mA

physical dimensions are closely related to the wavelenght of the signals. For practical purposes, this implies that an antenna generally will be bigger when designed for lower frequencies.

It is possible to divide antennas for UAS into groups and there are four usual types of antenna to be adopted for UAS:

a) The dipole antenna erected vertically is vertically polarised and requires a receiving antenna to be similarly polarised or a significant loss of signal strength will result [1];

b) The Yagi-Uda antenna contains only one active dipole element backed up by a number of passive, reflector elements which modify the basic radiation pattern to a predominantly directional beam with, however, small side-lobe radiations [1];

c) Parabolic dish antenna, as the name implies, are so formed, and as a pure parabola. By changing the disc diameter, for a given radio frequency, beams of various widths may be generated [1];

d) A square patch will produce an antenna with equal beam width in vertical and horizontal directions whilst beams of different width in the two planes will result from rectangular patches [1].

To describe the performance of an antenna, three major parameters should be considered [34].

Antenna Bandwidth

The fact that an antenna is designed for a specific frequency, or resonance frequency, does not mean it is unable to transmit or receive signals from other frequencies. Any antenna has a bandwidth which is the range of frequencies where the antenna is able to operate with acceptable efficiency [35]. To determine the bandwidth of an antenna, or how well they behave for a given frequency, there are different parameters. For example, the reflection parameter, which measures the amount of energy reflected by the antenna, is defined by the fact that if the antenna is perfectly matched with the transmitter, it will use 100% of the energy that the transmitter delivers. As this adaptation becomes worse (by the design of the antenna, or because the frequency to be transmitted is not the resonant one), the antenna will gather a lower percentage of the energy delivered by the transmitter. The spectrum frequency is summarized in Table 3.6. Like it was said before, UHF (300-3000 MHz), is required when covering large areas with little control over the receiving installation.

Band no.	Symbol	Frequency range	Wavelength	Corresponding metric subdivision of wavebands	Symbol
	ELF	<300 Hz	>1000 km		
3	ULF	300 Hz–3 kHz	1000–100 km	Hectokilometric	B.hkm
4	VLF	3–30 kHz	100–10 km	Myriametric	B.Mam
5	LF	30–300 kHz	10–1 km	Kilometric	B.km
6	MF	300 kHz–3 MHz	1 km–100 m	Hectometric	B.hm
7	HF	3–30 MHz	100–10 m	Decametric	B.dam
8	VHF	30–300 MHz	10–1 m	Metric	B.m
9	UHF	300 MHz–3 GHz	1 m–100 mm	Decimetric	B.dm
10	SHF	3–30 GHz	100–10 mm	Centimetric	B.cm
11	EHF	30–300 GHz	10–1 mm	Millimetric	B.mm
12		300 GHz–3 THz	1 mm–100 μm	Decimillimetric	B.dmm
13		3–30 THz	100–10 μm	Centimillimetric	B.cmm
14		30–300 THz	10–1 μm	Micrometric	B.μm
		300–3000 THz	1–0.1 μm	Decimicrometric	B.dμm

Note 1: band number N (N = band number) extends from 0.3×10^N to 3×10^N Hz
Note 2: prefix: k = kilo (10^3); M = mega (10^6); G = giga (10^9); T = tera (10^{12}); m = milli (10^{-3}); μ = micro (10^{-6})

Table 3.6: Frequency Spectrum up to 3000THz [22].

Antenna Polarization

There are two special cases of polarization: linear polarization and circular polarization. In a linear polarization, the electric field of the radio wave oscillates along one direction; this can be affected by the mounting of the antenna but usually the desired direction is either horizontal or vertical. In circular polarization, the electric field rotates at the radio frequency circularly around the axis of propagation [22]. It is best for the receiving antenna to match the polarization of the transmitted wave for optimum reception. Intermediate matchings will lose some signal strength, but not as much as a complete mismatch. A transmission from a circularly polarized antenna, received by a linearly polarized antenna (or vice-versa) entails a 3 dB reduction in signal-to-noise ratio as the received power has thereby been cut in half [22]. Fig. 3.6 shows the different possible polarizations for a propagation. When the field remains in a particular direction the wave is considered to be linearly polarized. In the case of circularly polarized antennas, the electric field rotates as it travels along. Elliptical polarization, on the other hand, is the polarization of electromagnetic radiation such that the tip of the electric field vector describes an ellipse in any fixed plane intersecting, and normal to, the direction of propagation [22].
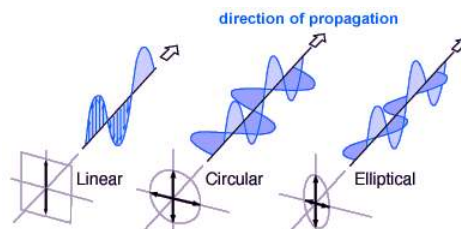
Figure 3.6: Types of propagation directions of an antenna [36].

Gain

Another important parameter that characterizes an antenna is the gain, or more correctly its directivity [34]. An antenna is a passive element, it has no gain since it does not amplify the signal. What it does is it concentrates the radiation to a certain area of the space. The higher the gain, the narrower the

beam of radiation. Using a moderate gain patch antenna (8 dBi) the radiation is concentrated in a beam of about 60°, covering a large area of flight. To increase the flight distance more gain is needed. This can be done using a 24 dBi parabolic antenna in which the beam width will be only 8° implying that the antenna has to be kept fully focused on the plane [22].

3.4.1 Tx Antenna Testbed Selection

High gain antennas for point-to-point communication links and UHF reception are usually Yagi-Udas, since parabolic dishes only become practical at the top end of the UHF band [22]. The ground station antenna will have to cover a wide range. Also, the bandwidth used for transmitting radio control will be between 430 and 490 MHz (amateur purposes). This is possible to do without spent a great amount of energy. It is just necessary the right antenna. A directional antenna concentrates all its energy into one direction allowing the same energy to go much further.

Regarding the gain of the antenna, when it is said that it is a high gain antenna (in this case, 13 dBi) this does not mean the transmission will "gain" something more or it is better. This just means the radiation pattern of this antenna, instead of a spherical shape will vertically look like an apple and, the higher the gain, the bigger the difference.

Another important aspect of this antenna, and antennas generally, is its polarization. In this case, it is linearly polarized. Theoretically, this will be a problem when the UAV is performing a manoeuvre like banking. However, the TSLRS receiver is already compensating with its diversity system. Since diversity is the feature that allows the receiver to choose, out of its antennas, the one with better reception a receiving antenna on the wing (horizontal) and another on the rudder (vertical) will solve this issue.

The A430S10 from Diamond Antennas [37] was chosen because it provides a bandwidth of 430-440 MHz with 13 dBi of gain and an aperture of 30° (Fig. 3.7(a)). Also, it is easily assembled and portable. Figure 3.7(a) shows the directivity chart for the A430S10: although it provides a narrow beam of 30° this will allow the UAV to fly long distances.

This type of antenna is widely used for UHF bands due to its moderate gain (which depends on the number of elements), linear polarization, unidirectional beam pattern with high front-to-back ratio. It is also lightweight and simple to build. It is priced at 79 € [34, 22].

(a) Directivity chart for the A430S10. (b) A430S10 antenna figure. (c) RC system, Thomas Scherrer wire antenna.
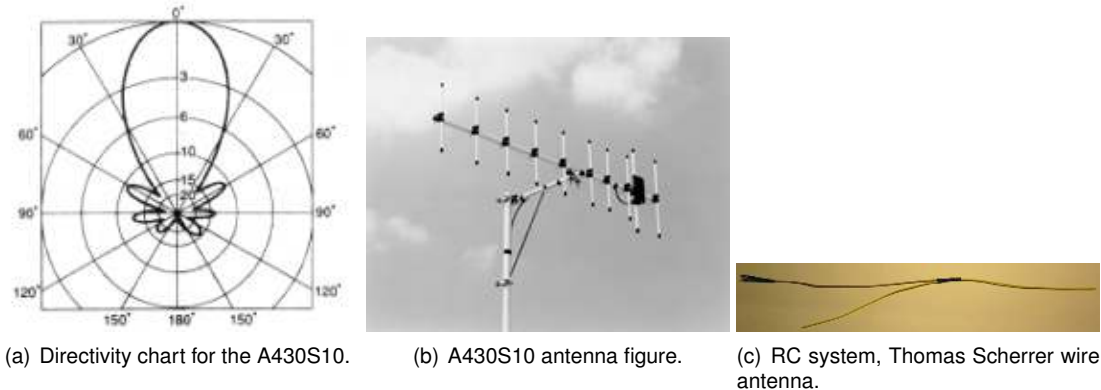
Figure 3.7: Long range RC system [37, 27].

3.4.2 Rx Antenna Testbed Selection

Omnidirectional UHF antennas used on mobile devices are usually short wires or rubber ducky antennas. Higher gain omnidirectional UHF antennas can be made of collinear arrays of dipoles and are used airborne. The type of antenna that comes standard with the Thomas Scherrer Receiver is linearly polarised. Figure 3.7(c) illustrates the antenna that comes with the Scherrer system.

However, simple as the antennas is, the ones which came standard were too small to take advantage of the diversity capabilities of the receiver, let alone be as separate from the video Tx as possible. For this reason, two new antennas were built. They are just the same as the one from Fig. 3.7(c) but extended. This was done making use of [38]. This way, one antenna was placed on the left wing (making it horizontally polarized) and the other on the vertical tail (making it vertically polarized).

3.5   Estimation for the Communication Link Systems

From [39], the IEEE 802.11 defines a mechanism by which RF energy is to be measured by the circuitry on a wireless link. This numeric value in an integer with allowable range of 0-225 called the Received Signal Strength Indicator (RSSI). It is not required that a vendor uses all 225 values, so each vendor will have a specific maximum RSSI value making the RSSI an arbitrary integer value that depends solely on the vendor. Nothing regulates the unit of measure of the RSSI, it can be dBm or mW. Regarding the strength of RF signals on the Scherrer device, RSSI sensors on board of the UAV are able to measure that across a range of frequencies. The signals, although noisy and ambiguous due to structural noise, allow estimates to be made of emitter locations. The RSSI output is an analogue voltage that reveals how strong the signal arrives to the receiver.

It is possible to predict the range of a transmission with the antennas in line of sight, without any obstacles with the Friis transmission equation [40]. This equation gives the power received by one antenna under idealized conditions given another antenna some distance away transmitting a known amount of power. The Friis equation states, given two antennas, the ratio of power available at the input of the receiving antenna (P_r) to output power to the transmitting antenna (P_t)

$$\frac{P_r}{P_t} = G_t G_r \left(\frac{\lambda}{4\pi R} \right)^2 , \tag{3.1}$$

where G_t and G_r are the antenna gains with respect to the isotropic radiator of the transmitting and receiving antennas respectively, λ is the wavelength, and R the distance between the antennas. The inverse of the factor in parentheses is called free-space path loss. The equation also has to consider a fade margin, which is a design allowance that provides for sufficient system sensitivity to accommodate expected fading, for the purpose of ensuring that the required quality of service is maintained. It was assumed that a 20 dB fade margin would suffice.

Table 3.7 provides the required data for calculating the range of the transmission. To calculate the range, the Watt unit was converted to dBm using Eq. 3.2, according to [22].

$$y[dBm] = 10 \log(1000x[W]) \tag{3.2}$$

	Monopole	Yagi
Frequency [MHz]	433	433
Output Power [dBm]	26.99	26.99
Sensitivity [dBm]	-113	-113
Receiving Gain [dBi]	2	2
Transmitting Gain [dBi]	3	13
Fade Margin [dB]	20	20
Communications Range [km]	56	160

Table 3.7: RC link range with both monopole and yagi antennas.

Knowing the frequency, *f*, it is possible to calculate the wavelength by Eq. 3.3, where *c* is the speed of light, which gives 0.69 m for both antennas with a 433 MHz.

$$\lambda = c/f \tag{3.3}$$

The range is given by Eq.3.1 or it can be calculated, adding the fade margin of 20 dB, by

$$Range[m] = 10^{(P_t + G_t + G_r + 20 \log_{10}(\lambda) - P_r - F_M)/20} \tag{3.4}$$

where F_M stands for fade margin. Equation 3.4, retrieved from [41], is valid for propagation in free space without obstacles and it gives the value of the received power on the antenna. Although these ranges are very optimistic because they do not consider interferences and obstacles, it is possible to conclude that, theoretically, the Yagi antenna will provide almost three times more range than the standard monopole antenna.

Chapter 4

Design of Video System

The aim of this chapter is to describe the design of the video system used for this dissertation in which Commercial Off-The Shelf (COTS) products are used. This includes the primary components such as the camera, video transmitter and receiver, On-Screen Display (OSD), also ground display and high gain antennas.

4.1   Remote-Person View Setup

Remote-Person View (RPV) is the method used for controlling a radio-controlled vehicle from the cabin's point-of-view. It involves mounting a small video camera and a video transmitter to an RC aircraft and flying by means of a live video down-link, commonly displayed on a portable monitor. As a result, RPV aircraft can be flown well beyond visual range, limited only by the range of the remote control, video equipment and batteries used.

A typical RPV setup makes use the following equipment, as depicted in Fig. 4.1:

- Camera;

- On-Screen Display (OSD);

- Video Transmitter (Tx);

- Video Receiver (Rx);

- Tx Antenna;

- Rx Antenna;

- Video Display;

- Video Recorder.

The following Subsections detail the characteristics and the selection of each component.
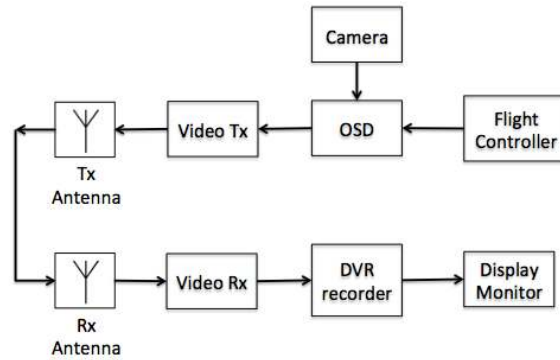
Figure 4.1: Scheme of the video system.

4.1.1 Camera

Most RPV cameras available today are primarily from the video surveillance and security industry and work very well for RPV due to its small size and low light capability. Plus, electrical wiring is exceedingly simple which is 3 wire outputs (ground, power and video signal output). Some may have an additional wire for analogue audio output if the camera also has a built-in microphone. Most cameras are designed to operate within a specific voltage range which is, usually, between 6 to 15 V making all RPV electrical components to operate with 2S and 3S LiPo packs without the need of voltage regulation (which is usually is made without great efficiency by losing energy in the form of heat) [42, 43]. When choosing the RPV camera, there are two primary variables to consider and three secondary more [44]:

- Image device type;

- Analogue video encoding type;

- Size;

- Field of view;

- Image definition.

Regarding camera imaging device, there are CCD or CMOS which stands for Charger Coupling Device and Complementary Metal Oxide Semiconductor, respectively. Typically, CCD type cameras have better low light and high light level performance meaning it will not go blind when pointing the camera into or near the sun and are, also, less susceptible to cause image wobble. Its disadvantages are weighting more, being bigger and more expensive and consuming more power when compared to the CMOS type [45].

About the camera video encoding type, either NTSC (National Television System Committee) or PAL (Phase Alternating Line) is, generally, not an important decision because most RPV components will support both types. With that said, the camera is, usually, the one video component in the system that is one or the other: PAL is the primary analogue video system used in Europe and does provide better resolution compared to NTSC but has a slower frame rate [44].

Many of the popular CCD FPV cameras used today make use of the 30 mm lens. Most cameras also allow to thread different mount lenses into the lens body tube to change the field of view (FOV) or even increase the light gathering capabilities, making them very adaptable.

The majority of these small cameras come with a standard 3.6 mm focal length lens giving about a 90° FOV. The lower the focal length number, the wider the FOV (fish eye effect). The higher the focal length number the more zoomed in the image will appear. A 3.6 mm, about 90° field of view is a good compromise in all aspects. However, in this aspect it is only a matter of preference some. Since this camera will be used just for flying and not for any particular application, the 3.6 mm lens will give a wide image with fish eye effect.

Regarding camera definition, within the 500 and the 700 TVL (TV lines of resolution) is what the average pilot uses. Of course, the more resolution the camera has, the more costly it will be.

Spec	Type
Imaging Device	CCD
TvLines	520
Encoding	PAL
Size	25x25 mm (1/3")
Consumption	50 mAh
Voltage	12 V
Weight	26 g
Price	76 €

Table 4.1: Kx-181 CCD Sony Camera characteristics [46].

With that said, the Kx-181 CCD Sony camera was selected because, as it can be seen in Table 4.1, it has the recommendable imaging device, CCD, 520 TVL and it is a fairly priced camera. The voltage range is within the 2S/3S batteries and comes with the, already stated, compromised 3.6 mm focal length lens.

4.1.2 On-Screen Display

An On-screen display (OSD) device allows the telemetry module of the flight controller (autopilot) to overlay information onto the video stream which can facilitate the its navigation. This information can include the UAV altitude, heading, direction to home, distance form home, velocity or power, etc.

There are many options when considering an OSD module. Most of the OSDs are designed to connect into its flight controller and get the information from there which is useful due to the fact that it is only needed a single add-on board in order to have OSD capabilities. Some flight controllers come bundled with an OSD built in. The most important thing to consider when considering an OSD is its compatibility with the chosen flight controller. All in all, what to look for in an OSD is:

- Weight;

- Price;

- Compatibility;

29

- Features.

In this segment, three OSD devices are analysed: the APM MinimOSD [47], the EZOSD [48] and the RangeVideoOSD [33].

The MinimOSD is a small circuit board designed and programmed by 3DRobotics that gets telemetry data from the APM flight controller and overlays it on the display monitor. To set it up, it is just a matter of hooking it up to the flight controller and connect it between the FPV camera and the video transmitter link. 12 V from a LiPo battery feeds directly the FPV camera and video transmitter. It also feeds the analogue line by a 5 V voltage regulator avoiding noises from servos attached to the APM. The Minim OSD is priced at 40 €. Features from the MinimOSD can be seen in Table 4.2 [47].

The RangeVideoOSD (RVOSD) is a stand-alone on-screen display (OSD) and flight controller. This is already the fifth generation which means there has been plenty of time to correct and improve this concept. The RVOSD enhances the overall flight experience through a continuous stream of information relating to the aircraft such as position, speed, altitude, distance from home and battery level. It performs the functions on a flight controller and an on-screen display in one compact package being, actually, lighter than the APM combination (it weights 29 g and the APM+OSD weights 35g). It contains four integrated sensors: two gyros, an accelerometer and a barometric pressure sensor that working together provide precise control of the aircraft under many different scenarios and even allowing six different modes. The RVOSD is priced at 240 €. Features from the RVOSD can be seen in Table 4.2 [33].

The EzOSD module may be used stand-alone and will offer navigation and basic voltage measuring capabilities. The 100 A current sensor records, not only the instantaneous current consumption, but also keeps track of battery level, recording precisely the energy (in mAh) consumed. Features from the EzOSD can be seen in Table 4.2.

	MinimOSD	RVOSD	EZOSD
Home Distance	✓	✓	✓
Home Direction	✓	✓	✓
Throttle	✓	✓	x
Speed	✓	✓	✓
Altitude	✓	✓	✓
Battery Status	✓	✓	✓
GPS coordinates	✓	✓	x
Pitch, row and heading angles	✓	✓	✓
Flight Modes	✓	✓	x
RSSI	✓	✓	x
Variometer	✓	✓	x
Artificial Horizon	✓	✓	✓

Table 4.2: Main Features of the OSDs considered : the MinimOSD, the RVOSD and the EZOSD [47, 33, 48].

Taking these comparisons into account, the MinimOSD is a viable choice since with its low price and provides has as many features as the RVOSD has. The EZOSD does not seem to provide Euler angles which, in case of using a camera gimbal, is absolutely necessary so that the pilot has a precise notion of the flight it is taking. Also, with the flight controller already chosen it is important not to have any compatibility issues and for the fact that it is a very popular item, it comes with a growing support

platform (MinimOSD-Extra) that is constantly improving it.

Figure 4.2: MinimOSD from 3DRobotics [47].

4.1.3 Video Transmitter and Receiver

With the use of analogue cameras (digital video systems being in an unaffordable price range), the RPV video system has to be an analogue RF system. They are fairly inexpensive, being mass produced and allow long ranges, when used with the appropriate antennas.

There are three main factors when selecting the video system [44]:

- Frequency;

- Output Power;

- Price.

Analogue wireless is the transmission of video and/or audio signals using radio frequencies which can be found in 1.2, 2.4 and 5.8 GHz as mentioned in Section 2.2

The COTS video systems market is offering a variety of light-weight mobile UAV to stationary GCS options with a wide spectrum of frequency bands available. However, each frequency has its own advantages as well as disadvantages which are briefly summarised in Table 4.3 and so, the 1.2 GHz frequency was chosen as a way to compromise long range with image quality since it will allow long distances with a fair video quality.

Frequency Band (GHz)	Pros	Cons
1.2-1.3	Signal range Penetration Less power consumption Clearer of interference	Antenna size 3rd harmonic of LRS
2.4	Video and sound quality Low cost system due to mass production	Expected interference in populated areas due to its wide use in cordless phones and wireless LAN Line-of-sight operational requirements Range affected by humidity in the air Legal transmitting power restrictions Interference with nearby RC systems
5.8	Small transmitting antennas Low distortions	Lowest Penetration Lowest Range Severe multipath distortion causes very poor performance in FM mode Line-of-sight operational requirements range affected by humidity in the air Equipment expensiveness

Table 4.3: Advantages and disadvantages of different frequency bands.

Regarding the power of the video transmitter, this will be listed in mW and it is not recommended to go over 1 W because, although it will give a better range, this will not be a proportional relation and it will, most likely, enable interferences with the GPS and the radio control. The large majority of RPV video Tx

also allow choosing between several different transmitting channels within its specific frequency band which allows the user to tune the video system for the best image transmission if one channel seems less noisier than the others.

	Partom	Lawmate	DJI - Lightbridge
Working Frequency [GHz]	1.2	1.2	2.4
Tx Output Power [mW]	850	1000	100
Rx Sensitivity [dBm]	-85	-85	-101
Weight (Air system) [g]	21	30	71
Video Encoding	PAL or NTSC	PAL or NTSC	PAL, NTSC or HDMI
Operating Current [mA]	245	350	700
Antenna Plug	SMA	SMA	MCX
Price [€]	83	137	1400

Table 4.4: Main specifications for each video system (Rx and Tx) [49, 50, 51].

There are two types of video systems here presented: digital and analogue. Table 4.4 presents two analogue systems: the Partom and the Lawmate and one digital: the DJI-Lightbridge.

Beyond the difference in output power and consumptions, the digital system allows a much more effective transmission: it is less affected by interferences and less susceptible to wobbling [22]. As it could not be, a system with much a higher quality, is much more expensive.

As it was said before, the video systems used for RPV are mass-produced. This mass-production is doe by many different companies but in a very generic way. For example, the two analogue receivers from Table 4.4 use that same Comtech module.

Whereas the quality of the 2 analogue systems is very similar in terms of performance, that the Partom weighs 9 g less and with 15% less output power there is a 30% reduction in consumption this leads to the conclusion that the Partom is more energy efficient. Also, it is less expensive than the Lawmate. For these reasons the Partom was selected. The complete system is shown in Fig. 4.3.

Figure 4.3: Video system developed by Partom.

4.1.4 Video Feed Antennas

With the video system and camera already chosen, the type of antenna is now narrowed down. The working frequency will be 1.2 GHz and, since the desire is to have long range, the ground station antenna will be a directional and high gain one. As for the onboard antenna, omnidirectional, circularly polarized antennas, usually, used because, for being circularly polarized, they naturally reject multipath

interference. However, an omnidirectional antenna is not famous for obstruction capabilities [22].

The chosen onboard antenna is a skew planar wheel antenna, shown in Fig. 4.4(a), which weighs 6 g, has a 2 dBi Gain and omnidirectional radiation pattern (see Fig. 4.4(b)). it is stated in [52] that combined with a helical antenna at the receiving end, it provides the desired long range (more than 50 km at 1.2 GHz) at a price of 35. €

(a) Figure of the skew planar wheel antenna.

(b) Skew planar wheel antenna radiation pattern (3D).
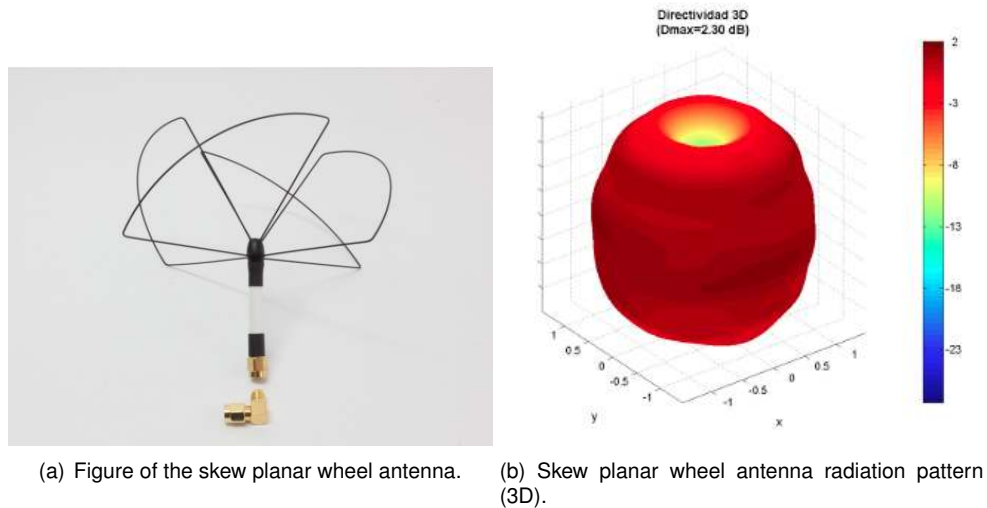
Figure 4.4: Skew planar wheel (SPW12) (1200-1360 MHz) Antenna [53].

The chosen ground station antenna is, thus a helical antenna sourced from Circular Wireless. It is a circularly polarized, directional antenna, with a gain of 12 dBi and 60° of beamwidth (see Fig. 4.5(b)), ideal for use in long range flights [52].The helical antenna is priced at 82 €.

(a) Figure of the helical antenna.

(b) Helical antenna radiation pattern (3D).
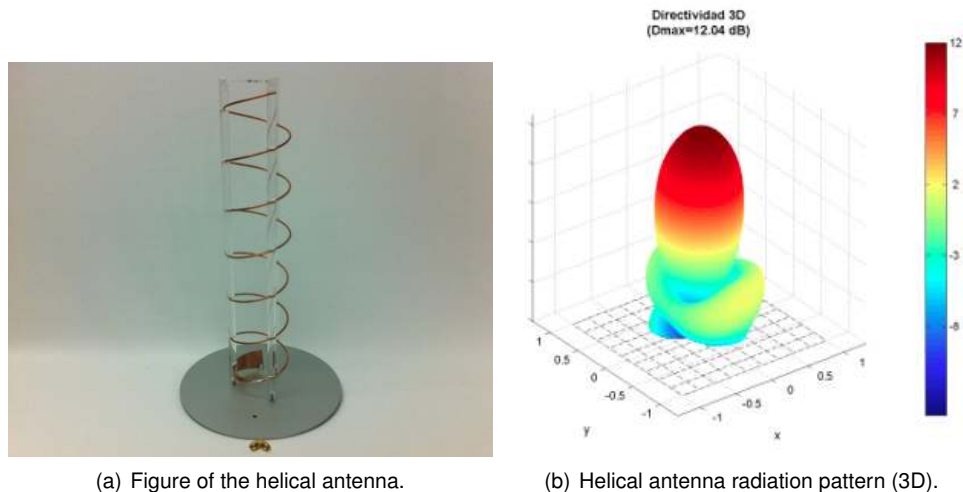
Figure 4.5: Helical 12 (910-1680 MHz) Antenna [54].

4.1.5 Video Display

For video display the Fieldview 1010, Fig. 4.6(a), was selected because it has an RCA input making it compatible with the video receiver and most importantly, it does not switch to "blue screen" when the

signal gets weak which on the contrary would represent a high flight risk. This display is priced at 165 €

(a) Fieldview 1010 Display Monitor [55].　　　　(b) DVR SD recorder [56].
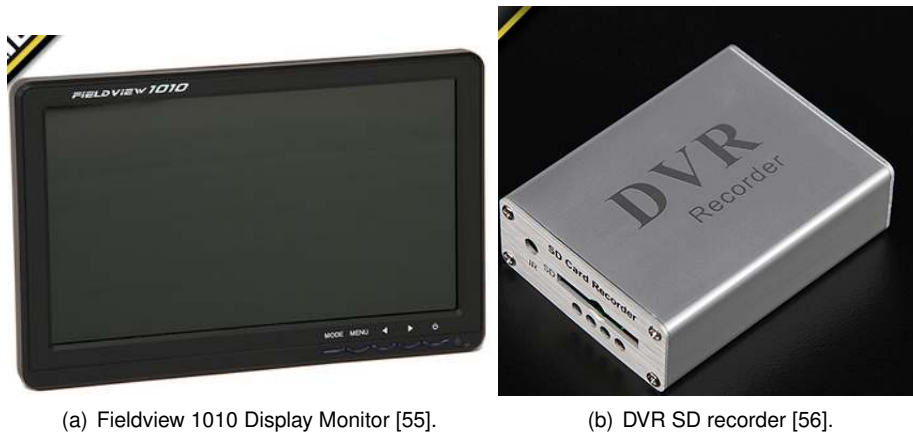
Figure 4.6: Recording and displaying devices.

4.1.6 Video Recorder

For video capture, the selected hardware was the Hobbyking DVR SD card recorder, Fig. 4.6(b). This recorder was supposed to arrive with a power supply that goes on the wall which did not come but a more practical solution was approached. Having an input voltage range of 5 to 30 V, a plug adaptor was made to connect it to a 3S LiPo battery which made the DVR a portable device.

With this device, 1.5 GB (Gigabyte) will record 1 hour of flight so, a 12 GB SD card will record the desired projects flight of 8 hours discussed in Section 1.3.

4.2 Propagation Aspects of Video Transmissions

Much effort has been made in recent years to develop objective image quality metrics that correlate with perceived quality measurement but only limited success has been achieved. Peak Signal-to-Noise Ratio (PSNR) coupled with the Mean Square Error (MSE) is the most used objective image quality metric, but they are, also, widely criticized for not correlating well with perceived quality measurements. The MSE, for practical purposes, allows to compare the true pixel values of the original image to the degraded image. It represents the average of the squares of errors between the actual image and the noisy image and it is proposed that the higher the PSNR, the better degraded imaged has been reconstructed to match the original image and better the reconstructive algorithm. However, the main limitation of this metric is that it relies strictly on numeric comparison and does not actually take into account any level of biological factors of the human vision system [57, 58, 59]. In [60], it is provided some insights on why image quality assessment is so difficult by pointing out the weaknesses of the error sensitivity based framework.

Equation 4.1 from [40], states that the only thing it can state is that if the received power is below the sensitivity value of the receptor, a connection is not possible. The contrary is not necessarily true but,

typically, if the received power is at least 20 dB above the sensitivity limit [41] it is likely that the video has a good reception quality.

$$\frac{P_r}{P_t} = G_t G_r \left(\frac{\lambda}{4\pi R}\right)^2 \tag{4.1}$$

In [61], a new approach on video quality metric based on light adaptation, luminance and chromatic channels, spatial and temporal filtering , spatial frequency channels, contrast masking and probability summation dynamics of light adaptation and contrast masking is attempted. It applies the metric to digital video sequences corrupted by compression artefacts and compared the results to quality ratings made by human observers. Although the results show improvements when compared to others, they also show systematic failure of prediction.

Since quantitative metrics for measuring video quality are still a long way from precise, the chosen method of evaluation for this dissertation is the subjective quality measurement, Mean Opinion Score (MOS), that has been used for many years and is documented by the International Telecommunication Union (ITU) in [62]. This method consists on using the human eyes to simply evaluate the video quality in different situations.

In the whole UAS communications, the video system is the most sensitive and so, the one that most suffers from disturbances. For this reason, in this section, it will addressed the various forms of disturbance in video transmissions.

Atmospheric Disturbances

The atmosphere can either increase the signal strength or weaken it. If the signal gets refracted as a result of changes in the refractive index occurring (especially within the first kilometres above the ground), it can travel beyond the line of sight of the pilot. However, if the changes in the refractive index are very abrupt due to weather conditions, the signals can be ducted by the ionosphere and be subject to multipath fading causing the distance over which the signal travels to be decreased.

Although multipath fading is necessarily accounted for in the design of video and communication systems, it can still be detected through the video link specially on a rainy day [22].

Polarization and propagation Losses

Even if considering that the path is free of losses, there is still a slow degradation of the signal quality since the power received is diminishing with distance. This is called propagation loss. A horizontally polarized wave is weakened more rapidly by travelling over the ground than a vertically polarized wave. While the polarization of sky-waves (waves that do not follow a path always near the ground) usually vary, sometimes quite rapidly, and splits into several components that follow different paths, ground waves usually retain the polarization characteristics they had when they left the antenna. As a rule, a vertical conductor radiates a vertically polarized wave and the same goes for a horizontal one [22].

The performance of a receiving antenna is improved if it can be oriented to take advantage of the polarization of the incident wave. If possible, both vertically and horizontally polarized antennas should be tried. This means that if the transmitting antenna is vertically polarized (in a vertical position) and the receiving antenna is tilted 90° relative the the transmitting antenna then, theoretically, there will be

a total loss by polarization.This is called polarization loss. When a circuit produces mostly surface-wave propagation, it is important that the antennas at both ends of the path have the same polarization. However, vertically polarized antennas provide most effective surface-wave coverage. A propagated ground wave takes three separate paths to the receiver: direct, ground-reflected and surface wave, as shown in Fig. 4.7 [22].
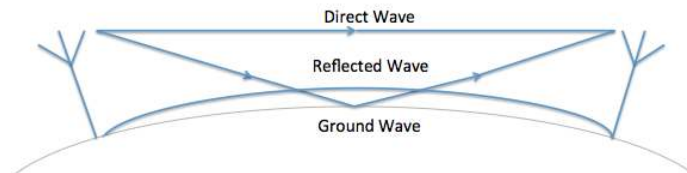
Figure 4.7: Types of Wave Propagation.

When both transmitting and receiving antennas are close to the ground, the direct and ground-reflected paths tend to cancel each other while the intensity of the surface wave diminishes in strength when increasing height. Its intensity becomes negligible at about 1 wavelength over ground and 5 to 10 over sea water. The best type of surface for surface-wave transmission is sea water. The electrical properties of the terrain that determine the attenuation of the surface-wave field intensity are very little.

Omnidirectional antennas are not isotropic and typically have nulls in their radiation pattern, aligned with the antenna axis. If the Tx antenna is somehow pointing to the Rx antenna, the effective gain of the Tx is much lower and this effect will add extra loss to the video link. The most common situation of antenna radiation pattern null is when the UAV is flying over the GCS [22].

Chapter 5

Setup of the Unmanned Air System

5.1 Setup of the RPV Airframe

Turning a RC plane into an UAV implies putting a flight controller between the RC receiver and the aircraft's servos, so that it sends telemetry data through the OSD and the pilot can orient himself through the monitor display and to enable the autopilot function so that the flight controller can take over control when the pilot desires so.

5.1.1 APM 2.5 Between the Rx and the Servos

Channel	TSLRS	APM
1	Throttle	Ailerons
2	Ailerons	Elevator
3	Elevator	Throttle
4	Rudder	Rudder
Autopilot	6	8

Table 5.1: Connections between the APM and the Rx700.

The way the APM 2.6 is connected is to plug female-to-female cables from the RC receiver into the APM inputs and plug the servos (and motor controller) into the APM outputs. Table 5.1 shows how the female-to-female cables should be connected: the ground (black) wire of each connector should be on the outside, closest to the edge of the board. Each channel that the pilot wants the APM to control should be connected to the corresponding input on the APM board. An extra pin was activated in the Scherrer's Rx to manipulate the autopilot function, Channel 6. This channel will allow the pilot to change between manual and automatic flights by controlling the PWM value. As for the output pins, the way to plug the servos and other devices for the APM to control is shown in Fig. 5.1: the ailerons are attributed to pin 1, the elevator to pin 2, throttle to pin 3 and rudder to pin 4.

Figure 5.1: 4 Channels plane setup [63].

The flight controller must be facing forward, the GPS connector should also face forward. The board must also be right side up (Fig. 5.2(a)), with the Inertial Measurement Unit (IMU) shield at the top. It is important that it is attached with velcro to the airframe and mounted on a solid platform, as seen in Fig. 5.2(b), so that it does not move around during flight, be as close as possible to level when the plane is in its flying orientation and, also, it would have to be as close to the center of gravity as possible because that is where the vibration is the least. It is also necessary the supplied APM Power Module for the power source and the Electronic Speed Controller (ESC) to power the servos and motor as seen in Fig. C.2 from Appendix C.
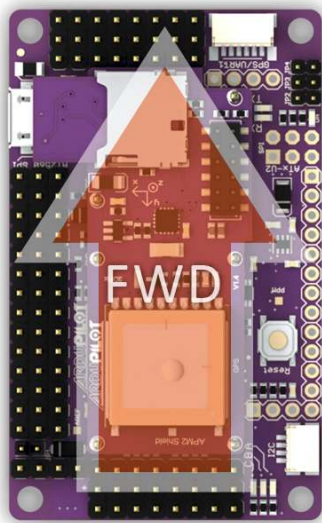
(a) Direction of the APM with the aircraft [64].
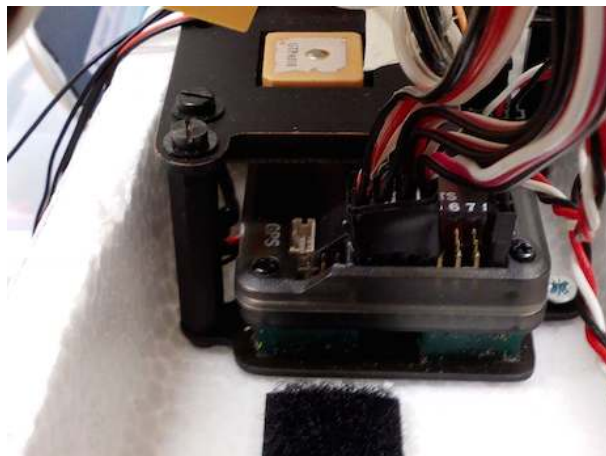
(b) APM attached with velcro to the airframe.

Figure 5.2: Concerns about the mounting of the APM.

5.1.2 Flight Controller Configuration

Before using the APM, it has to be configured first which is done through Mission Planner (MP) and for that there has to be a properly setup RC transmitter (Tx) and receiver (Rx) pair. The configuration process starts by uploading the latest firmware into the APM which, in this case, is the arduplane firmware.

The port assigned to the APM has to be *Arduino Mega 2560* and the Baud rate set to 115200.

Clicking on 'Connect' button, the MP will connect via MAVLink which is a protocol for communicating with small unmanned vehicle [29].

Since the Skywalker is a standard airframe, a pre-made configuration file can be used [63] but there is still the need to configure it for the hardware in question, which is done in MP with the button 'Calibrate Radio'. The results should then match Table 5.2:

Channel PWM	Low	High
Ch 1:	Roll left	Roll Right
Ch 2:	Pitch forward	Pitch back
Ch 3:	Throttle down(off)	Throttle up
Ch 4:	Yaw left	Yaw right
Ch 8:	Manual	Autopilot

Table 5.2: Radio Calibration End Result.

Figure C.2 from Appendix C shows a detailed connection scheme of how the RC sub-system was assembled.

5.1.3 MinimOSD Setup

The MinimOSD is a small circuit board that gets telemetry data from the APM flight controller and overlays it on the FPV monitor. To connect the MinimOSD to the APM 2.5 a 5-pin splitter cable is used. The connections shown in Fig. 5.3 are required.
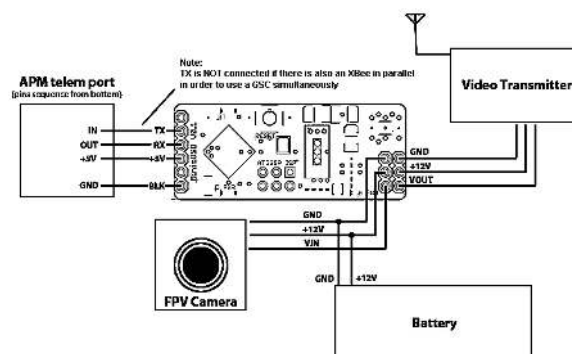
Figure 5.3: MinimOSD between the APM and Video Transmitter Schematics.

Regarding the setup of the MinimOSD, it is based on two components: a processor and a video chip. From the digital side, the flight controller is providing MAVlink data to the OSD processor allowing it to parsing and packaging. Then, the video chip overlays the data onto the video stream outputting it to the camera.

It is possible connect the MinimOSD to the computer and load its firmware. For this it is necessary an FTDI cable and download its respective driver so that the computer recognises the FTDI cable. Both the FTDI and the OSD have 6 pins so the only thing of concern when connecting the two is just putting the Vcc together (5 V with 5 V).

To configure the OSD there are a couple of programs that need to be downloaded: the MinimOSD Config. Tool as well as the binaries that contain the firmware. MinimOSD-Extra [65] is a developer

website that is concerned with extending the features and functionalities of the MinimOSD. Here it is possible to access the source code if there is the need to configure some extra feature like, for example, for getting RSSI from the control receiver. The firmware for the MinimOSD in this particular case is the 'MinimOSD-Extra_Plane_Pre-release _2.4_r719.hex' while the configuration tool is the 'CT Tool for MinimOSD Extra 2.3.2.0 Pre Release r727.zip'. Inside the .zip file there is an executable file that automatically runs ConfigTool. The first step is to enable this function in the APM so that it can communicate with the MinimOSD-Extra as it was explained in Subsection 5.1.2. After the firmware update, the character set (a .mcm file) comes next (for the character set both sides of the MinimOSD have to be powered: one side from the USB port and another from the video pins with a 3S LiPo battery).

For this dissertation, an important feature of the OSD is the RSSI output. The RC receiver, the Scherrer Rx-700, has an extra output pin on channel 12 for RSSI out. This pin will send a voltage of 2.2 V when the connection is at 100% and 1.1 V when it is at 0%. As shown in Fig. 5.4, this spot was soldered to a pin so that Ch12 becomes a 4 pin channel. Two wires are, then, connected to the APM: the RSSI and ground as it can be seen in Fig. 5.4. For the APM to recognize the RSSI in, it has to be configured in the Mission Planner (MP). The way to do this is to connect the APM to the MP, next go to the $Config/Tuning$: $StandardParams$ menu, search for the 'Receiver RSSI sensing pin (RSSI_PIN)' parameter and set it to the desired port number (in this case A1).

Figure 5.4: APM reads RSSI from Ch12 to channel A1.

When using the MinimOSD, as in this case, there is the need to setup the APM to communicate with it and there are a few requirements that need to be met, in order to be able to use the MinimOSD-Extra (which is the programme that allows the configuration of the MinimOSD). The data stream rates have to be configured correctly and to do so the EEPROM parameters on the MP have to be according to Table 5.3. These parameters are configured through the Full parameters list in the in the Config/Tuning tab.

Parameter	Value	Description
SERIAL_BAUD	57	Telemetry output at 57600
SR1_EXT_STAT	2	Extended status stream rate to ground station
SR1_EXTRA1	5	Extra data type 1 stream rate to ground station
SR1_EXTRA2	2	Extra data type 2 stream rate to ground station
SR1_EXTRA3	3	Extra data type 3 stream rate to ground station
SR1_POSITION	2	Position stream rate to ground station
SR1_RAW_SENS	2	Raw sensor stream rate to GCS
SR1_RCCHAN	5	RC Channel stream rate to ground station

Table 5.3: EEPROM parameters for the interaction between APM and MinimOSD.

Although the APM already recognizes the RSSI output, the MinimOSD has to be recalibrated via

MinimOSD-Extra so that on the screen it outputs the correct signal strength in percentage. This is done in the Config. Tool in a few steps presented below. Fig. 5.5 shows the window where this can be done.
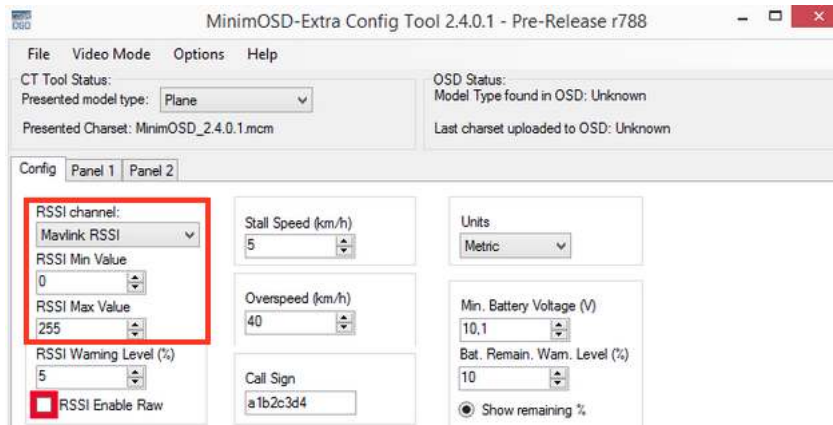
Figure 5.5: Configuring the MinimOSD to correctly read the RSSI values.

- In Config. Tool check the 'RSSI Enable Raw' check-box so that when the OSD is powered up with the APM, the raw values are seen, and check if the RSSI channel is set to 'MAVLink RSSI';

- After the APM has booted up and with the RC Tx is working, the screen will show the raw value that, after, has to be set in the 'RSSI Max Value' box;

- With the RC Tx turned off, it will then show the raw value that has to be set in 'RSSI Min Value';

- Plug the OSD to the FTDI cable again and uncheck 'RSSI Enable Raw' check-box and change the Max and Min values (230 for Max and 150 for Min).

5.1.4 Video Transmitter Setup

The video transmitter is connected to the MinimOSD and powered through the Easy FPV board. When connecting a 3S LiPo battery to the Easy FPV board, it will not only power the Video Tx but also one side of the MinimOSD and the camera. Table 5.4 expresses the connections from the MinimOSD through the Easy FPV board to the Video Tx. The auxiliary Figure in the table shows the shape of the Easy FPV board. A detailed scheme of the referred connection is shown in Fig. C.1 from Appendix C.

Port nr.	MinimOSD	Miniboard input	Port	Miniboard output	FPV Tx
1	Vout	Vout	1 Yellow	Video in	Video in
2	12V	12V	2 Red	Power 12V	Power 12V
3	GND	GND	3 White	Audio in	Audio in
			4 Black	GND	GND

Table 5.4: Connections from the MinimOSD through the miniboard to the video Tx.

As it was done in SubSection 5.1.2, Fig. C.1 from Appendix C shows how the RPV system was connected for the realization of this dissertation.

5.2   Setup of the Ground Station

5.2.1   Control Station Setup

The first thing to do when using a long range system is to bind the remote controller with the LRS system. In this particular case, a Graupner mc-24 (remote-controller) was coupled with a Scherrer transmitter. While the mc-24 works with a 2.4 GHz transmitter, the Scherrer Tx700 will make the controller work with a 433 MHz one which allows the UAV to be controlled at long distances.

The binding process is described in the user's manual [27] so there is no need to repeat it in here. However, there is an exception with the Graupner mc-24 that is not mentioned: the remote control has to receive a PPM signal from the mono jack end tip and ground from the base as seen in Fig. 5.6(a). So, the wire is cut which in fact is three wires (PPM, Ground and Power) and the mono jack is welded as seen in Fig. 5.6(b).

(a) From stereo to mono adaptation for the mc-24.   (b) Mono jack transformation.
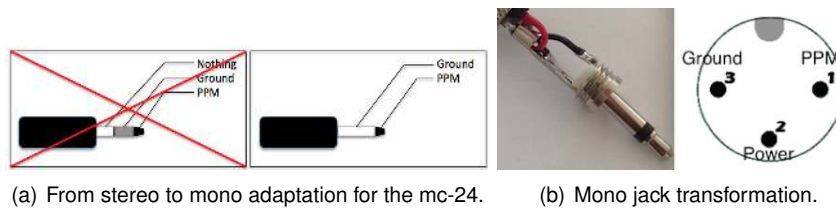
Figure 5.6: Graupner mc-24 coupling with Scherrer Tx.

The connections were made and the binding procedure was done (the receiver confirming it with a fast blinking mode and the transmitter with a permanent red light on). The ground control station is, then, composed by the radio control transmitter, the long range transmitter (TSLRS Tx700) and a suitable antenna, as illustrated in Fig. 5.7.
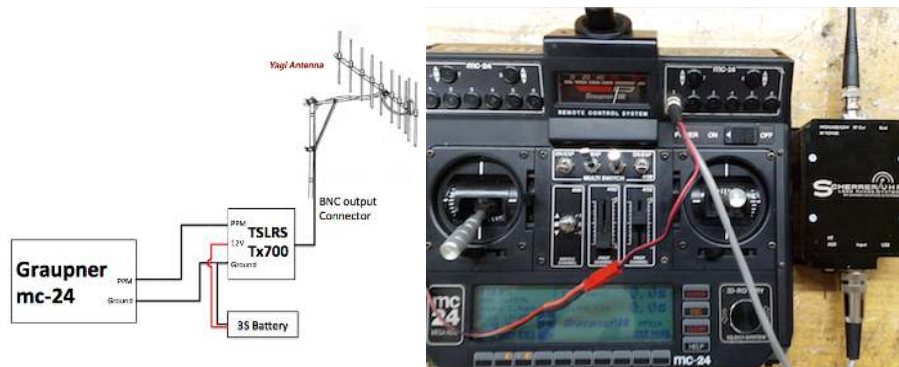
Figure 5.7: Control station connection schematic.

5.2.2   RPV Station Setup

The RPV ground station is composed by a video receiver and suitable antenna, a digital video recorder and a LCD monitor, as illustrated in Fig. 5.8. These components have an operating voltage of 7 to 18 V (LCD screen), 5 to 30 V (DVR) and 7 to 12 V (video receiver) and so, they will all be powered by a 3S

LiPo with 4200 mAh capacity. Figure 5.8 shows a scheme of how the ground station is powered. Since the video receiver will be attached to the helical antenna it must be placed far away from other devices and the control antenna not to be affected by external interferences.
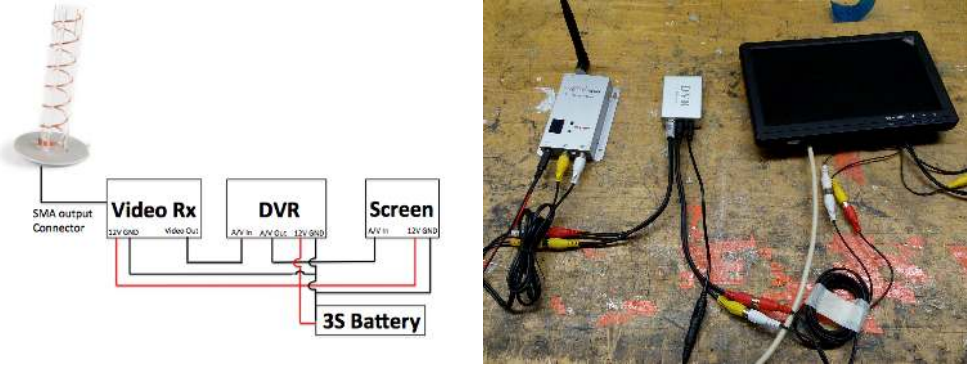
Figure 5.8: RPV station connection schematic.

Figures 5.9 show the final result for the UAS setup on the day of the first flight.

(a) UAV.

(b) Ground station.

Figure 5.9: Final result for the UAS setup on the day of the first flight.

Chapter 6

Sub-Systems Testing in Controlled Environment

To certify the COTS products that were purchased, "black-box" testing was used.

Black-box testing is the method used for certifying COTS equipment that is acquired. The fundamental of this technique is to test the functionality of the component without any understanding of the internal structure of the component.

UAV flight operations are limited in range and endurance by the mission's essential communication link capabilities.

In this section, it will be addressed the multiple-fold problem of trading off in a set of mission requirements, balancing between the communications capabilities and the desired UAV radius of action. The system will be first evaluated in a controlled environment in the sense that it is being hold by a person two meters above the ground in seven discrete positions where there is no risk to the UAV or the surroundings.

6.1 Testing of the Radio-Control Link Systems

6.1.1 Test Design

The objective of this test is to evaluate the influence of the type of antenna in the control system range and also the influence of the output power in a single radio-link configuration. Figure 6.1 shows the two antenna configurations that are going to be tested. six configurations total are, then, evaluated by varying the output power of the transmitter (0.5, 1 and 2 W) and by switching the antennas (Monopole and Yagi).

Section 3.5 shows how the RSSI can be used as a measure of the signal since it relates signal strength with distance. In this particular test, the RSSI is retrieved by the Mission Planner with a PC, as shown in Fig. 6.2, where it is given as a percentage (0% means there is no signal between the GCS and the UAV and 100% means maximum strength).

(a) Output power test using the Monopole.   (b) Output power test using the Yagi.

Figure 6.1: Radio-link system configurations.

In order to test the control system without the Telemetry Radio system, the ardupilot APM, which interprets the RSSI signal from the Rx, has to be connected to the PC via USB port. In an actual flight, it is not possible to have the PC connected directly and so this value is sent to the OSD that gives the RSSI value overlaid on the flight video.

Figure 6.2: Mission Planner reading RSSI out.

The place of choice to perform the experiment was Cascais because it allowed the portable device to travel 8 kilometres without obstacles, as seen in Fig. 6.3.

Figure 6.3: Points along the coast where the Radio control experiment took place.

This experiment was done along its coast, with the GCS installed at the Marina of Cascais and the portable device consisting of the RC components to be later installed in the UAV travelling along the 8

kms. Including the 0 km mark, the measurements took place in seven discrete places as labeled in Fig. 6.3. The test proceeded the following steps:

1. Mount the Ground Control Station (which includes the Tx700, the Graupner mc-24 and the battery) and the portable configuration (which includes the ardupilot, Rx700, servo, Power Module, battery and PC);

2. Test the system at 0 km and turn off both batteries;

3. Go along the coast from Fig. 6.3, turn on the equipment at the first checkpoint, measure the RSSI level and move the servo to its extreme positions;

4. Turn off the equipment, change the transmitter antenna from monopole to Yagi and turn on the equipment, measure the RSSI level and move the servo to its extreme positions;

5. Repeat steps 3. and 4. for checkpoints 2 to 10. The experience stops when the servo no longer responds continuously.

6.1.2 Test Results

Distance (km)		3.95		6.97		8.32	
	0.5W	✓	✓	x	x	x	x
Monopole	1W	✓	✓	x	x	x	x
	2W	✓	✓	x	x	x	x
	0.5W	✓	✓	✓	✓	x	x
Yagi	1W	✓	✓	✓	✓	✓	x
	2W	✓	✓	✓	✓	✓	✓
		Margins	Contin. Mov.	Margins	Contin. Mov.	Margins	Contin. Mov.

Table 6.1: Output behaviour of the servo in function with the distance.

Table 6.1 shows how the servo behaved in terms of movement continuity (Contin. Mov.) and reaching its end positions (Margins) in each checkpoint for the six possible antenna configurations.

Since both configurations only started showing signs of weakness at km 7, the table begins at the previous checkpoint and ends at km 8 due to the fact that the coast started retrieving thus, imposing obstacles to the transmission.

From Table 6.1 it is possible to see that, regarding the monopole antenna

- The connection ends between 4 and 7 km;
  -It is noteworthy that between these checkpoints the connection breaks no matter what the output power is. It suggests that output power on the monopole does not make any difference;

- It has a range of, at least, 4 km.

and regarding the Yagi antenna

- The signal gradually loses its strength from the 7 km checkpoint;
  -Using different output powers it is possible to see the gradual decrease from the 7 km to the 8 km mark;

- The maximum registered range is at 8 km;
  -However, with 1 W the servo was still moving going for its extremities but at an inconstant pace. While with 2 W the servo started moving continuously towards its margins. This means that the maximum range is, at least, 8 km;

- While the monopole handles 4 km, the Yagi antenna doubles the range of the connection.

(a) Changing output power on the Monopole antenna.　(b) Changing output power on the Yagi antenna.
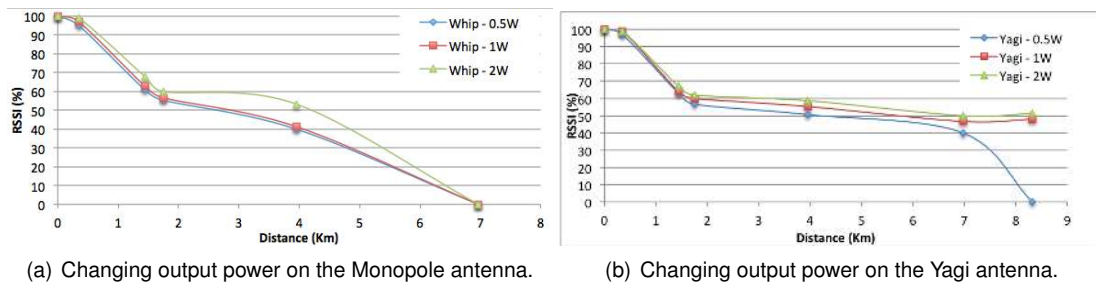
Figure 6.4: Changing the output power and antennas of the transmission.

Figures 6.4 show the obtained values for RSSI, which measures signal strength in percentage, at a certain checkpoint for each antenna configuration.

Figure 6.4(a) reports the evolution of the RSSI for the monopole antenna as a function of distance.

- Different output powers show similar results;
  -An output power of 0.5 W will handle the same range as the 2 W and spend less energy;

- The system handles a distance of, at least, 4 km.

Fig. 6.4(b) reports the evolution of the RSSI for the Yagi antenna as a function of distance

- Different output powers show similar results until the 7 km checkpoint is reached;
  -At the 7 km checkpoint with 0.5 W, the RSSI falls 10 points and no longer works at the last checkpoint;

- From 0.5 to 1 W the signal regains its strength;
  -With a distance of 8 km, the RSSI is still strong and only decreased 10% from 1 km to 8 km. Although the last checkpoint still has 40% signal strength, the experiment ended due to lack of space as previously discussed;

- Between the 2 last checkpoints there is an increase in RSSI;
  -This is due to the directivity of the Yagi antenna. Since the UAV was already out of sight it got harder to manually orient the antenna towards the same.

In conclusion, although using a directional (the Yagi) antenna will give double the range of an omni-directional (monopole), a new factor emerges: the antenna has to be manually oriented. Also, the use of more than 0.5 W as output power is only justified at an 8 km distance. The estimates that were done are very conservative due to the fact that these tests are performed 2 m above the ground. When flying at 1000 m altitude better results are expected.

6.2   Testing of the Video Link System

6.2.1   Test Design

The objective of this test is to evaluate the influence of the type of antenna used for the video link in its quality and range as shown in Figs. 6.5.

(a) Vertical (GCS) - Vertical (UAS).

(b) Vertical (GCS) - Skew Planar (UAS).

(c) Heliaxial (GCS) - Vertical (UAS).

(d) Heliaxial (GCS) - Skew Planar (UAS).
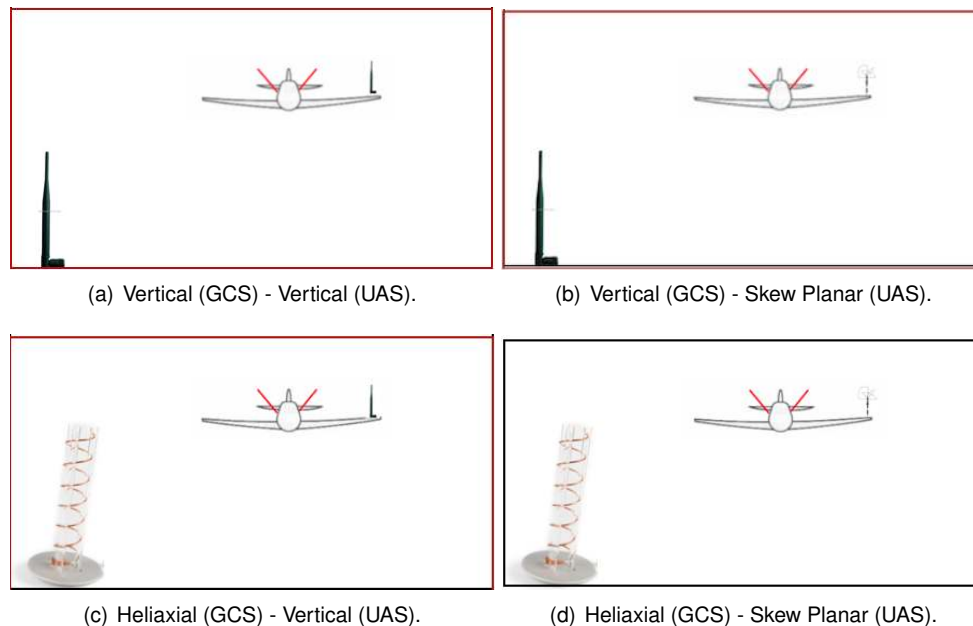
Figure 6.5: Video-link system configurations.

For these tests a small platform was built using the following equipment:

- Partom 1.2 GHz, 850 mW transmitter;

- Standard omnidirectional with linear polarization antenna;

- Partom receiver with the same omnidirectional with vertical polarization antenna;

- Circularly polarized skew-plan wheel antenna;

- Circularly polarized helical antenna.

The first step when testing the video system is to understand the different issues that weaken the video link quality and, then, to replicate them in order to determine if any adopted solution corrects those

issues. When analysing video quality, it is important to have in mind a few issues that often occur with video systems and they are:

- Propagation loss;

- Polarization loss;

- Antenna radiation pattern null;

- Signal obstruction.

These issues are mentioned in Section 4.2 where it is explained how it is possible to replicate them and this is what was tested with the various antennas configurations. Table 6.2 indicates how, in theory, these problems can be solved.

Video Issues	Proposed Solutions
Multipath	- Circular polarization: naturally rejects multipath as the polarization change from left hand to right hand with signal bounce - Diversity: at the receiver end. Two antennas at the transmitting end with a separation of at least one wavelength from each other.
Propagation Loss	- Higher gain antenna - More transmitting power - More receiver sensitivity
Polarization Loss	- Circular polarization: will give no polarization losses - Diversity at the receiver end, with one antenna vertical and the other horizontal.
Radiation Pattern Null	- Diversity: at the receiver end. Two antennas at the transmitting end with two video transmitters tilted 45 deg relative to each other.
Signal Obstruction	- Diversity: at the receiver end. Two antennas at the transmitting end with two transmitters working in different frequencies placed in both wing tips (this way the probability of obstruction is much smaller)

Table 6.2: Proposed Solutions for multipath fading, propagation and polarization losses, radiation pattern null and signal obstruction [66].

Currently, the available equipment does not allow the testing of all these proposals since there is only one transmitter available and there is no diversity equipment in the video system and so, the proposed solutions from Table 6.2 that involved more than one video equipment or diversity system are not tested. However, this table can be used as a future reference.

Secondly, it is important to state which parameters will be varied for this test:

- Distance;

- GCS antennas;

- UAV antennas.

With these four antennas, it is possible to make four different antenna configurations in each checkpoint.

Thirdly, a location that provides the same range as for the communications link is selected. The location of Cascais was found to be too noisy for an analogue video system (for the RC link was a digital one which is less affected by noise). So, Fig. 6.6 shows the new place of choice in which the testing took place: Baleal, Peniche.
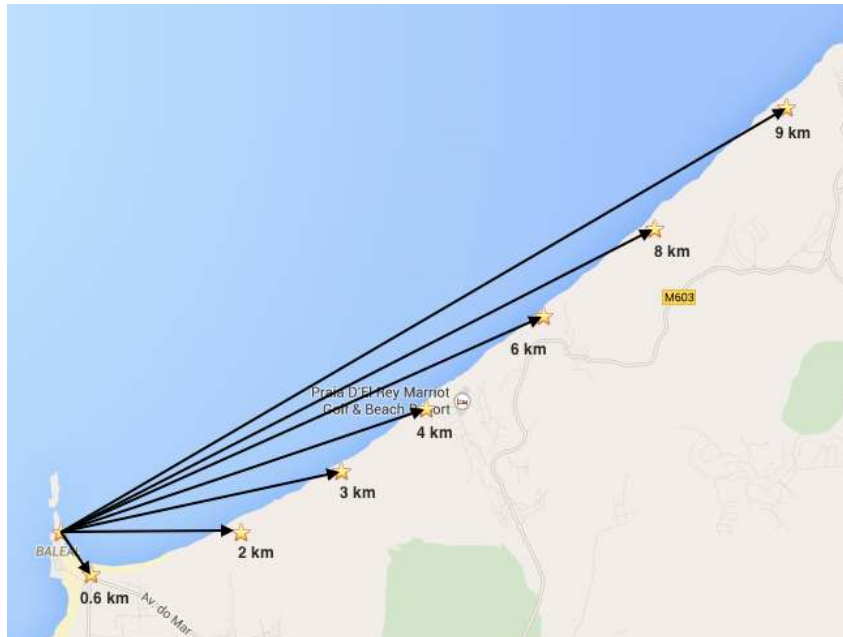
Figure 6.6: Points along the coast where the experiment took place.

In this test, are shown the differences between vertical and circular polarisation, a higher and a lower gain antenna and how these different solutions can solve issues from Table 6.2. The video sequences were shown to a group of 4 random people who, according to MOS in [67] compared the various samples.

Lastly, for the testing of propagation loss, 6 different parameters were taken into account [67]:

- Image colours;

- Image contrast;

- Image borders;

- Movement continuity;

- Flickering;

- Smearing.

With these evaluation parameters and the different video shots from each checkpoint and each antenna configuration, the video quality was evaluated in terms of colour, contrast, borders and movement continuity on a 10 point scale from bad to excellent while flickering and smearing were rated also with a 10 point scale but from very annoying to not annoying.

6.2.2 Test Results

Regarding propagation losses, Fig. 6.7 illustrates how video quality is affected by the distance between operating antennas according to the subjective opinion data gathered. The same figures show that:

- Flickering and smearing are the ones that most affect the quality of the video and the ones that are most affected by propagation loss (the increase in distance);

- When different polarisation is used from each side, the image quality tends to get worst Specially regarding flickering and smearing, so it is advisable to use antennas with the same polarisation.

(a) Vertical (GCS) - Vertical (UAS).

(b) Vertical (GCS) - Skew Planar (UAS).

(c) Heliaxial (GCS) - Vertical (UAS).

(d) Heliaxial (GCS) - Skew Planar (UAS).
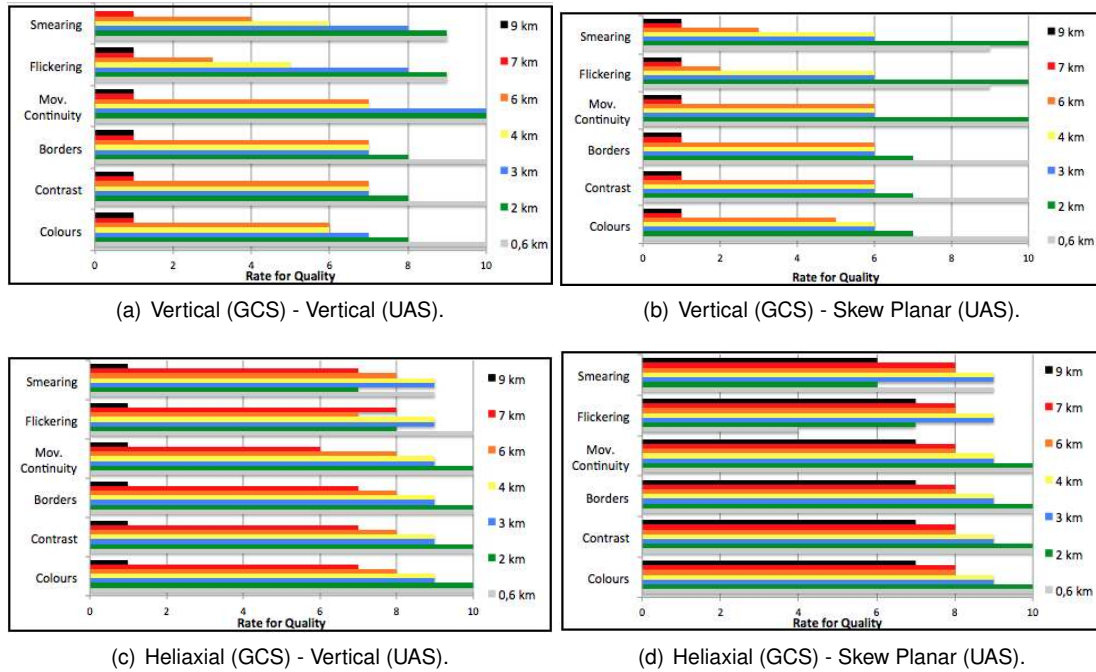
Figure 6.7: Effect of propagation loss in video quality.

Contrast, colours and image borders seem to be equally affected by the distance and so video can be classified by a generalized parameter, an overall image quality. The points attributed to the these parameters where used to build an average score. A representation of that evaluation in shown in Fig. 6.8 where the overall video quality is rated as a function of distance.

Regarding Figs. 6.7 and 6.8 there are several things that are noteworthy:

- The best configurations have the Helical on the GCS since good video quality goes much further in range;

  -This may be due to the fact that the receiver, for having a higher gain antenna, is concentrating its focus into a more specific area and can interpret the signal much easier. More specifically, the system works best if the helical is coupled with the Skew Planar because they have the same polarisation;

- The configuration with the vertical antenna on the GCS and the skew planar onboard seems to be the worst;

  -For having different polarisations, it is the one where the connection is the worst and totally losing it at the 6 km mark;

- The maximum range is 7 km;

-The limit in range for the video system is determined by the helical-skew configuration at 7 km. The last tried checkpoint was at 9 km where the connection did not show any signs.
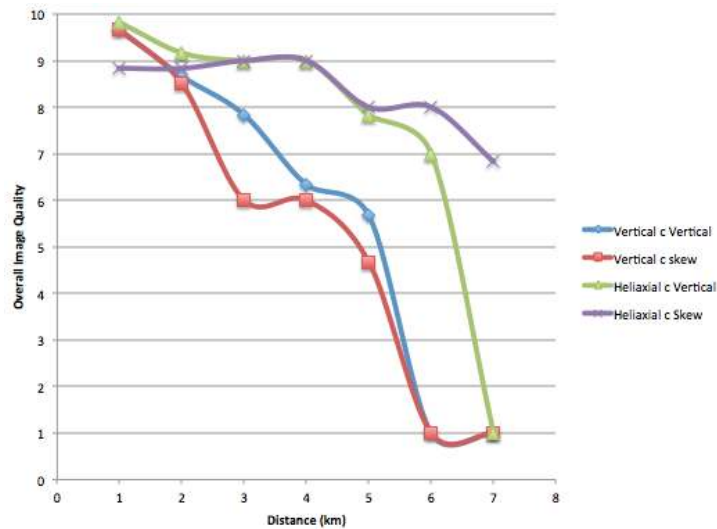
Figure 6.8: Video Quality affected by propagation loss.

Regarding the video issues discussed in Section 4.2, as the distance between antennas grew, their presence became stronger and stronger.

Tables 6.3, 6.4 and 6.5 illustrate the effect of different antenna configurations on signal propagation issues where V, v, H, s stand for vertical antenna mounted at the GCS, vertical antenna onboard, helical antenna on the GCS and skew planar antenna mounted onboard, respectively. They also show how much these issues degrade the video link as a function of the distance. This classification was also attributed using a mean opinion score, same as the rate of image quality for propagation loss. The minus signs, '-', indicates that the image was beyond annoying.

Inclination

Distance (km)	V-v	V-s	H-v	H-s
0.6	7	8	9	9
2	4	8	9	9
3	4	3	9	10
4	2	1	8	9
6	-	-	8	8
7	-	-	-	5
9	-	-	-	-

Table 6.3: Inclination with different configurations and distances.

Regarding inclination, the antenna configuration that is most affected is, clearly, the monopole antennas. This is because when the GCS is always in a vertical position, and so, with vertical polarisation, the onboard monopole antenna is changing polarisation from vertical to horizontal, thus affecting the link quality (see Table 6.3).

On the other side of the spectrum, the helical with skew planar antenna configuration, for having both circular polarisation, is the less affected configuration by the inclination of the UAV; however, it can be seen that with the increase in distance the effect starts showing some signs of weakness (see Table

53

6.3).

Pattern Null				
Distance (km)	V-v	V-s	H-v	H-s
0.6	8	9	8	9
2	1	3	7	7
3	1	1	9	9
4	2	1	4	9
6	-	-	1	7
7	-	-	-	3
9	-	-	-	-

Table 6.4: Antenna pattern null with different configurations and distances.

With respect to the antenna pattern null, it is seen that both configurations with vertical polarisation in the GCS are greatly affected by the pattern null, showing that the gap on top of the radiation shape is large and easy to find. Thus, with this configuration it is not advisable to fly the UAV over the GCS. As for the Helical configurations, it is seen that this gap is difficult to find although it increases with distance (see Table 6.4).

Obstruction				
Distance (km)	V-v	V-s	H-v	H-s
0.6	7	7	10	7
2	1	1	7	7
3	1	1	3	5
4	2	1	2	4
6	-	-	1	1
7	-	-	-	1
9	-	-	-	-

Table 6.5: Obstruction with different configurations and distances.

The case of obstruction, is the one that affects the link in most ways: if using a vertical polarisation in the GCS, the signal drops less than 1 km away and even the helical configuration starts breaking at a distance of 3 km (see Table obstruction).

In conclusion, the best configuration for a long range flight is a circular polarisation with high gain antenna at the ground station. The circular polarisation will overcome banking and obstructions and the high gain antenna will allow coverage of a farther flight. However, having a directional antenna will increase the risk of losing link suddenly because of the reduced aperture angle. The UAV will have to be flying almost in a straight line for it not to break the link. For this problem, an antenna tracker would solve the issue since this device tracks the transmitter and points the ground station antenna to where the UAV is. As for the obstruction, although the circular polarisation seems to correct the issue, a diversity device could correct it permanently. As said in Subsection 6.1.2, the estimates that were done are very conservative due to the fact that these tests are performed 2 m above the ground. When flying, at 1000 m altitude better results are expected.

6.3   Testing of the Telemetry Radio

The telemetry radio allows the connection of the ardupilot APM via MAVlink to the computer. It allows the user, for example, to modify the mission while the UAV is still in the air.

The purpose of this test is to check if the long range RC system (LRS) and the telemetry radio, for working in the same frequency, interfere with one another. Another objective of interest is to access the telemetry radio connection range. Summarizing, this test is divided into two experiments, as shown in Figs. 6.9: one that tests the range of the telemetry radio and another that tests the interference of both 433MHz system on each other.

(a) Range test.   (b) Interference with RC system.
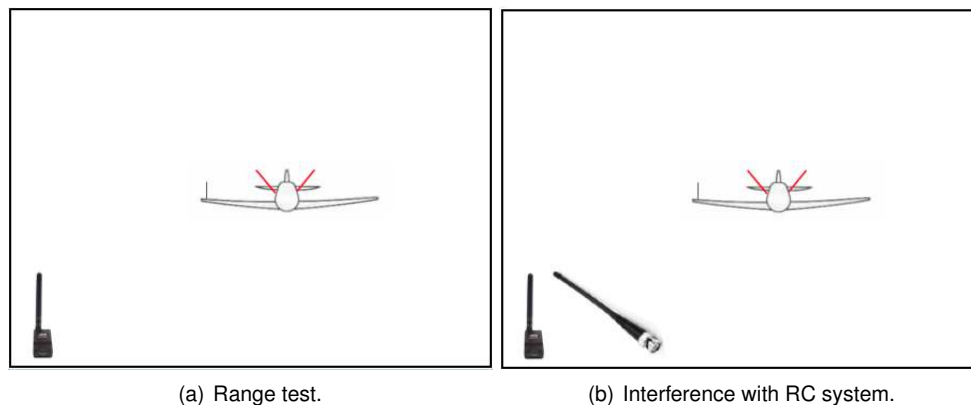
Figure 6.9: Tests of telemetry radio.

6.3.1   Testing of the Telemetry Radio range

For this test it is used the same route as in Fig. 6.3, the same used for testing the communication system. The equipment is composed by:

- Telemetry radios and antennas (onboard and ground station);

- Computer;

- Ardupilot APM.

The procedure for this experiment is the following:

- The APM is connected to the telemetry radio (TR) and then it is powered through the power module;

- The ground station TR is connected to the PC through an FTDI cable (the corresponding driver has to be installed otherwise the PC will not recognize the COM port);

- In the main page of the Mission Planner the two radios are connected;

- The RSSI is appointed in the 'Flight Data' menu in the HUB windows as shown in Fig. 6.10;

- This is done at every checkpoint until the link goes down.
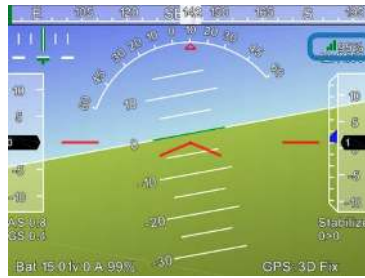
Figure 6.10: Test of the telemetry radio-link system configurations.

Checkpoint	Intensity of Connection	90 deg Inclination	Distance (km)
#1	99%	97%	0
#2	97%	89%	0.36
#3	0%	0%	1.5
between 2 and 3	44%	42%	0.85

Table 6.6: Link Quality from the telemetry radio which is read on the Mission Planner HUB.

The telemetry radio was proven to be the weakest link in the whole system mainly, because of two reasons: the antenna used (a linearly polarized monopole) and the operating power (100 mW). As it can be seen in Table 6.6, the link shows a strong connection in the first two checkpoints but rapidly loses signal after 800 m. However, it is noteworthy that a 90° inclination almost does not affect the strength of the link because, in the video link, the monopole antenna is strongly affected by its inclination.

6.3.2 Testing the Interference between the Telemetry Radio and the TSLRS

For this test it is also used the same route from Fig. 6.3 and it is composed by the same equipment as in Subsection 6.3.1. First, the receiver is included on the onboard equipment and the standard monopole antenna is connected. Secondly, the monopole is replaced with the Yagi to evaluate the quantitative difference.
This experiment is done in two different points: at 0 m, a desk test, and at 360 m.

Table 6.7 represents the interference between the two systems. As it can be seen, the TR triggers no interference on the LRS due to its low output power of 100 mW while the LRS transmits a minimum of 500 mW.

Checkpoint	LRS on TR/touch (monopole)	LRS on TR/touch (Yagi)	TR on the LRS
#1	from 99% to 60%	from 96% to 54%	x
#2	from 97% to 20%	from 91% to 30%	x

Table 6.7: Influence of the LRS on the telemetry radio.

On the other hand, the LRS can affect the TR if the antennas are touching each other or if the LRS is emitting 2 W and they are very close together.

The Yagi, having the transmission directionally channelled has more influence on the telemetry transmission. However, it can also be seen that if the antennas are reasonably away from each other, the interference is almost null.

In conclusion, although the TR is the weakest sub-system for the desired long-endurance flight, it can still be a useful tool. Supposing an electric UAV powered by solar panels, the TR allows the user to make changes to a predefined mission without having to land it. It will just have to be in loiter mode in a 1 km range. This reduces the risk of damaging the UAV when landing.

6.4   Testing the Interaction between Video and Communications Systems

The objective of this experiment is to evaluate the interference between the communications link and the video link. First, it is important to understand why this test is useful. On one hand, the onboard video system emits strong RF signals in its primary frequency and also in other frequencies (there is usually noise from spurious emissions). These RF emissions can greatly affect the link of surrounding equipments such as RC receiver, GPS receiver, stabilization systems and servos. On the other hand, GCS wise, the same goes for the RC transmitter. Its third harmonic can affect the video link quality; if the noise produced is too high, it will interfere with the video system that works on the same frequency of the RC's hamonics.

The main causes for video link interfering with other systems are itemized below:

- Video Tx output power;

- Video Tx antenna position.

As for ground station interferences, in the case of the TSLRS in binding mode (0.5 W at 432.3 MHz), the 3rd harmonic appears at 1296.9 MHz with -65 dBm, [25]. Table 6.8 shows how these two frequencies can interfere. The right frequency will provide the best video quality possible using these two systems.

3rd harmonic	Scherrer	3rd harmonic 1296.9	All signals contain harmonic frequencies. Some waveforms contain large amounts of energy at harmonic frequencies. Bad designed transmitters emit more energy at harmonic frequencies
	Partom	Rx Frequency 1080 1120 1160 1200 1240 1280 1320 1360	

Table 6.8: Principle cause for RC Tx interference with video Rx.

Summarizing, for this experiment, it is important to see if all the systems are compatible and find out their limitations. For that, the experiment will be divided into two sections: ground station interferences and onboard interferences.

6.4.1   Ground Station Interferences

RC Tx with Video Rx

On the ground station there is a video receiver and a radio control transmitter. In terms of interferences, there is only one way in which they can happen: the RC transmitter may interfere with the video

receiver. The objective of this test is to evaluate, in the same way as in Section 6.2, the interference of the RC Tx in the video system. For this test, the equipment used is:

- Video ground station (Rx, antenna, LCD and DVR);

- RC transmitter and antenna;

- Video transmitter.

The location for this test is the same as seen in Fig. 6.6 and only the circularly polarized antenna (helical with skew planar) configuration will be analysed as shown in Fig.6.11 a).
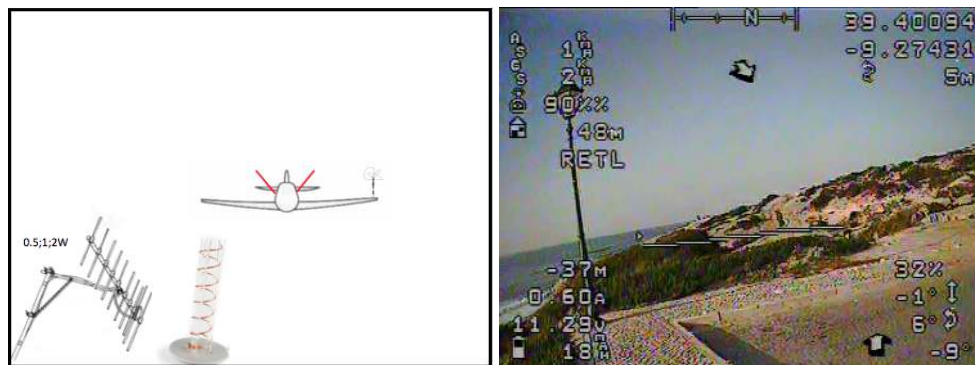
(a) Ground station interference with varying output power.

(b) Evaluation outlook of the experiment.

Figure 6.11: Ground station interferences and outlook.

For the last checkpoint, when the video reception is the weakest, the video system will be tested in its eight available frequencies, in onder to find what the combination with less interferences is. Besides, it will be important important to know if the video signal has a shorter range than the RC, because the video signal degrades progressively and the RC can simply stop working. It will be an extra warning that the UAV is getting out of range.

Thus, in this section, different aspects will be tested:

- Video interferences;

- Video frequency planning;

- Range.

For this test, two extra components will be added:

- MinimOSD;

- APM 2.5.

This way it will be possible to evaluate the signal strength through the RSSI as explained in Subsection 6.1.1. Figure 6.11 b) exemplifies the outlook of the evaluation.

With the same evaluation parameters from Section 6.2 and the different video samples from each checkpoint, video quality was evaluated rating colour, contrast, borders and movement continuity just as in Section 6.2.

Regarding propagation losses, Figs. 6.12 illustrate how video quality is affected by the distance between antennas and the difference between using only the video system or all the systems together according to the subjective opinion data gathered.
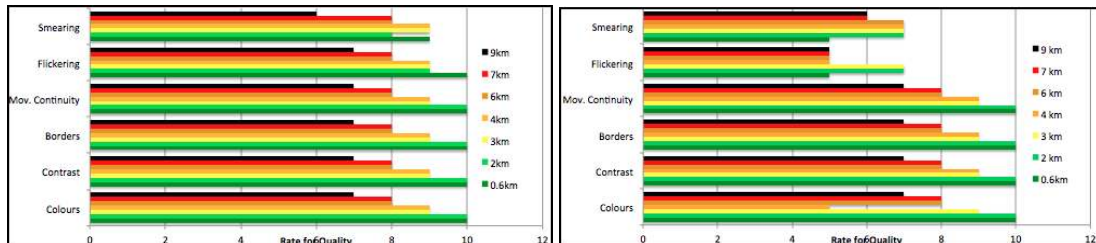
(a) Video Quality according to the presented parameters in 6.2.

(b) Video Quality when added the APM and the Mini-mOSD.

Figure 6.12: Ground station interferences and outlook.

Figure 6.13: At a distance of 8 km, with only the video system (circularly polarised configuration).

(a) GCS turned off.

(b) GCS turned on.

Figure 6.14: Video System coupled with the onboard RC equipment.

As it was done in the video alone quality test, an overall parameter was built based on the six parameters from Figs. 6.12 and the result was compared with the overall video quality of the video system alone which can be seen in Fig.6.15.

As it can be seen, the video quality of the UAV becomes degraded when compared with the results of the UAV from Fig. 6.12. At first, it was assumed that this was due to the interference of the control
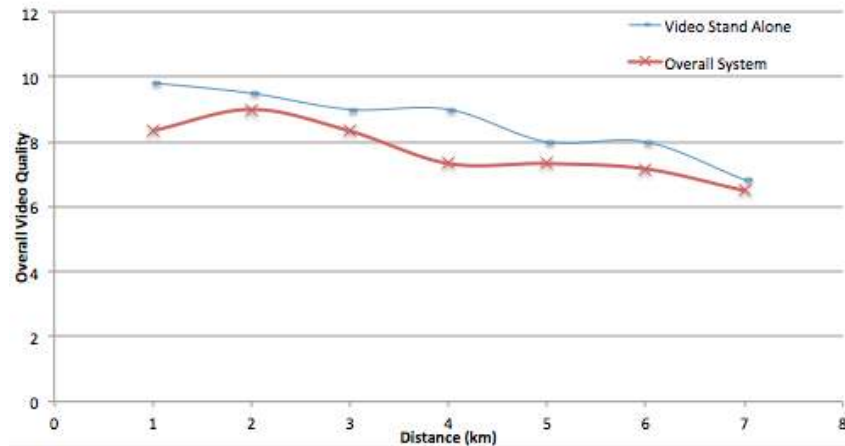
Figure 6.15: Comparison between the overall video quality in standalone and installed configurations.

transmission. However, when the RC Tx was turned off on the last checkpoint the video quality did not improve, as it can be seen in Fig. 6.14. It stayed with the same smearing and flickering it had before. By comparing Figs. 6.13, 6.14 and 6.15 one can visually check the above mentioned.

Frequency Planning

Regarding frequency planning, the evaluation of video quality corresponding to each video frequency was done the same way as in Section 6.2 but in the form of a table.

	at 6000m							
Ch. Freq.	Ch. Nr.	Colours	Contrast	Borders	Mov. Continuity	Flickering	Smearing	AVQ
1080	4	4	4	4	4	4	4	4
1120	5	3	3	3	3	3	3	3
1160	6	5	5	5	5	5	5	5
1200	7	8	8	8	8	8	8	8
1240	8	8	8	8	8	8	8	8
1280	9	8	8	8	8	8	8	8
1320	H	7	7	7	7	7	7	7

Table 6.9: Evaluation of video quality depending solely on the transmission frequency.

It can easily be seen from Table 6.9 that from channels 7 to 9 there seems to be not much of a difference and that they are the best channels to be transmitting on. it is important to say that, channel 8 is the closest from the Scherrer's 3rd harmonic thus, it can be said that there is no interference. However, there are other unrecognised noise sources that heavily degrade the system near the 1120 MHz frequency.

Concluding, there was the expectation that the RC ground system would cause interferences in the video ground station but this experiment showed a different kind of interference: the video system is affected by the overlaying panels. The use of the MinimOSD adds noise to the video. Also, the recommendable channel to be transmitting on is between 7 and 9, including. It is, also, noteworthy the fact that the entire experiment was performed with the RC system with 2 W of output power so that the hypothetical interference was as strong as possible.

6.4.2 Onboard Interferences

The objective of this test is to evaluate the interference of the onboard video Tx on the onboard receiving equipments: GPS, ardupilot APM and TSLRS Rx.

The equipment used is

- Video Tx and antenna;

- APM Ardupilot;

- GPS;

- Radio-Control Rx;

- Servo.

The place in Fig. 6.6 is again used for the onboard interferences test. From Section 6.1 the maximum distance that the monopole antenna signal can travel with 0.5 W is between 4 and 6 km.

Video Tx with GPS

Regarding the interference of the video Tx on the GPS receiver, a simple test was performed. The video Tx antenna was right next to the GPS and, for 1 minute, the GPS coordinates, from Mission Planner, were retrieved as it is shown in Tables 6.10 and 6.11. The values were written with both the video Tx on and off.

Time (s)	Real Latitude (°)	GPS Latitude (°) (off)	GPS Latitude (°) (on)
10	38.737298	38.737311	38.737311
20	38.737298	38.737298	38.737312
30	38.737298	38.737332	38.737307
40	38.737298	38.737341	38.737315
50	38.737298	38.737257	38.737309
60	38.737298	38.737299	38.737334

Table 6.10: Obtained GPS latitude with video transmitter off and on.

Time (s)	Real Longitude (°)	GPS Longitude (°) (off)	GPS Longitude (°) (on)
10	-9.136955	-9.136892	-9.136943
20	-9.136955	-9.136955	-9.136937
30	-9.136955	-9.136898	-9.136937
40	-9.136955	-9.136897	-9.136925
50	-9.136955	-9.136926	-9.136917
60	-9.136955	-9.136917	-9.136919

Table 6.11: Obtained GPS longitude with video transmitter off and on.

Table 6.12 shows that the reading of the GPS has an error associated with the receiving data. However, that error does not seem to be aggravated with presence of the video transmitter.

Concluding, with this test there seems to be no interference of the video Tx on the GPS receiver.

Video Tx with RC Rx

Regarding the RC receiver, it was necessary to check if the onboard video transmitter was interfering with the RC Rx. For this, the whole system was used so that the MinimOSD would state the value of the RSSI on the ground station screen, as explained in Subsection 5.1.3.

Time (s)	Video Off (m)	Video On (m)
10	5.7	4.4
20	0.0	2.2
30	6.2	4.4
40	6.9	3.8
50	5.2	5.8
60	3.3	3.9

Table 6.12: Read distance from real UAV position with transmitter off and on.

Figure 6.16: Outlook of the test for the Interferences of the Communications on the Video System.

First, Table 6.13 shows the testing of the the servos in the same way as in Section 6.1 for movement continuity and the ability the reach their endpoints.

	Distance	0 km	0,6 km	2 km	3 km	4 km	6km	8 km
	0.5W	✓	✓	✓	✓	✓	✓	✓
Yagi	1W	✓	✓	✓	✓	✓	✓	✓
	2W	✓	✓	✓	✓	✓	✓	✓
		Margins	Contin. Mov.	Margins	Contin. Mov.	Margins	Contin. Mov.	

Table 6.13: Testing the performance of the servos as done in Section 6.1.

Secondly, the values of the RSSI were written down for every checkpoint, as done in Section6.1 with and without the video system turned on. The results in Table 6.14 are the same from Section 6.1 and Table 6.15 has the results obtained for the whole system bundled.

	Yagi	0km	0,35km	1,5km	2km	4km	7km	8km
	0.5W	100	97	63	57	51	40	0
RSSI (%)	1W	100	99	64	60	55	47	48
	2W	100	99	67	62	59	50	51

Table 6.14: Testing the performance of the communications system on the Yagi configuration without the video system as in Section 6.1.

	Yagi	0 km	0.6 km	2 km	3 km	4 km	6 km	8 km
	0.5W	97	95	95	93	92	92	84
RSSI (%)	1W	97	96	96	95	95	95	87
	2W	97	97	97	97	97	97	90

Table 6.15: Testing the performance of the communications system on the Yagi configuration while the RSSI is provided by the video link.

As it can be seen, the results retrieved with the whole system are, clearly, better then the ones retrieved with the RC standalone. While the first table, at km 8, with 0.5 W has 0% of RSSI, using the

RC standalone platform since the second, at 8 km is still showing a strong signal of 84%. This can be due to the change in environment or antenna directivity. Opposed to what was said in Section 6.1, the RC system despite being digital is still affected by the area where it is transmitting in.

Concluding this segment, there seems to be no interference of the video Tx onto the RC receiver. The experience stopped due to lack of space. It is important to say that the video transmission end before the RC which is desirable as previously stated.

6.4.3   Pan and Tilt Testing

Figure 6.17: Camera gimbal setup.

Regarding the implementation of the pan and tilt servo-mechanism of the video camera, it was tested in two ways: first, if it responded to the assigned channels and secondly, if it would automatically stabilise (if it would respect a predefined floor). After trial and error calibration in Mission Planner's initial setup menu (Fig. 6.17), the values for maximum and minimum servo limits were found and are shown in Table 6.16. Table 6.17 represents the obtained response to the RC controller where the minimum limit for tilt was raised so that the camera would not touch the canopy.

	Maximum	Minimum
Pan	2100	1100
Tilt	2100	1600

Table 6.16: Servo limits of the pan and tilt.

	-180°	180°	Mov. Continuity
Pan	✓	✓	✓
Tilt	✓	✓	✓

Table 6.17: Performance checks of the pan and tilt.

After positive response from the RC commands the stabilise box was checked. This would order the camera to respect and follow the attitude defined by the accelerometer. In this test, the tilt responded with success. However, the pan would only respect a heading that pointed North, since the UAV was laying on the ground. After this test, it was decided that the tilt was ready for a flight test. However, the pan did not respond well to the test and could cause disturbances to the system

It is suggested that the autonomous tracking is used on a second camera gimbal (a second video system) whose purpose is not to pilot the UAV but to monitor the surroundings.

6.5 Testing of the Energy Consumption

6.5.1 Test Design

The components electrical energy consumption is one of the elements that limit the range and endurance of the UAS. Depending on how much time the batteries last, the UAV will be able to fly longer or shorter distances.

In this setup, both components from the ground station and the onboard use batteries for energy and so it is important to do an estimate of how much they consume and how long they last. Thus, the objective for this test is to do an estimate on the consumption of each component and for this two experiments will be made: the consumption of the RPV ground station (receiver, DVR and screen) and the onboard video transmission (Tx, OSD and camera). As for the control system, both ground station and onboard will be tested.

Only a simple static test to the APM and RC receiver was done because their energy consumption depend on too many variables, for example, the type of flight operation (if it is in manual or automatic control) how much use it is given to the servos, etc. For this test, a wattmeter is coupled with the system in each experiment.

6.5.2 Test Results

Regarding the engine, when choosing a battery, it is recommended that the current of the battery exceeds that of the motor. This ensures that even if the motor is running at 100 % the battery does not hold it back.

The motor current is calculated as follows:

Maximum power of motor = 328 W

Battery voltage (LiPo 3S) = 11.1 V

Maximum motor current = 328/11.1 = 29.55 A.

A battery pack with current discharge rating above 29.55 A is therefore needed.

For a three cell LiPo battery pack chosen with the following specifications,

Battery capacity = 4.2 Ah.

Maximum Discharge current = 45 C.

Battery Maximum discharge current = 189 A.

it is seen that the amperage of the battery well exceeds that of the engine and so it is suitable for the design.

For each test the components were evaluated (through a Wattmeter) in Voltage, Amperage, Wattage and accumulated energy consumption (in mAh). Table 6.18 shows how each sub-system behaved with a 3S LiPo battery with 4200 mAh capacity.

As it was expected, changing antenna does not affect the energy consumption, with the exception of the radio control transmission: the monopole antenna is consuming too much energy. It was tested and

Component	Total Test Time (min)	Current (mA)	Energy (mAh)	Avg. Input Power (W)
Video Rx (Heli)	45	770	825	9.43
Video Rx (Monopole)	45	770	825	9.25
Video Tx (Skew)	60	3100	3069	35.81
Video Tx (Monopole)	60	3100	3060	35.81
RC Rx (Wire)	60	240	245	2.96
RC Tx (Yagi,Low)	30	220	128	6.09
RC Tx (Yagi,High)	30	710	370	6.09
RC Tx (Monopole,Low)	30	650	307	6.09
RC Tx (Monopole,High)	30	222	900	5.61

Table 6.18: Sub-systems testing in energy consumption.

the antenna was not in short-circuit. The reason why this was happening was not found (it was tested if the antenna was in short-circuit). Assuming that each battery is equally charged at the beginning of each testing, the video reception is the one that spends the most amount of energy both in the ground station and onboard. Onboard, the video system is, mostly, responsible for the energy consumption maybe due to the fact that the video transmitter is very inefficient, since it loses too much energy from heating.

From this sub-systems testing, it is possible to conclude that, with a 4200mAh battery, it is not recommendable to perform RPV for more than one hour. This value, will obviously be drastically reduced by the electric engine: at full throttle, a 10"x5"' blade will drain the battery in little over five minutes (see Table B.6). A more accurate estimate for total system consumption can be done with actual flight tests.

Chapter 7

Flight Testing

When changing from a controlled to a free environment where the UAV is going to fly, the most important thing is to minimize possible errors. The first set of variables is weather conditions. In here, there are two that can kill the mission: strong wind and precipitation. Strong wind can change a stable flight into a total disaster; rain, on the other hand, (not to talk about electricity and water) can greatly affect the video quality by the sudden and multiple changes in the refraction factor causing multipath interference, as mentioned in Section 4.2. Updated weather conditions were retrieved from websites [68] and [69] where it is possible to obtain wind speed, gusts and direction, temperature and humidity.

Before each flight it is important to check, as in Fig. 7.1, if the UAV is giving the correct GPS coordinates and if the distance home is nearby because in case of permanent link loss the UAV will head for the predefined 'Home'. When the UAS is turned on, the GPS will lock this location as 'Home'. It is also important to check the servos response and battery charge.

Figure 7.1: GPS lock is an important pre-flight check.

7.1 Short Range Flight Test

Before a long range flight, the link quality was studied, first, with short range flight tests. One of those flights is analysed here. The chosen date for this flight test corresponded to favourable weather conditions, as specified in Table 7.1.

The flight test was conducted at *Pista de Aeromodelismo de Corroios*. This provided a safe place where the pilot could test all the actuators of the UAV and test climb, cruise, banking, loiter, descent and

67

Condition	Value
Wind velocity (km/h)	15
Gust (km/h)	20
Direction	West
Temperature (^{o}C)	14-18
Humidity (%)	55

Table 7.1: Weather conditions during short range flight test.

finally landing. The goal of this test was to perform a simple flight where RPV system was installed, so that the pilot could perform the whole flight by looking at the screen and data could be retrieved.

7.1.1 RC Link Quality

The pilot performed a manual flight around the track and the values for RSSI were retrieved to see the variations in RSSI within a maximum range of 340 m.
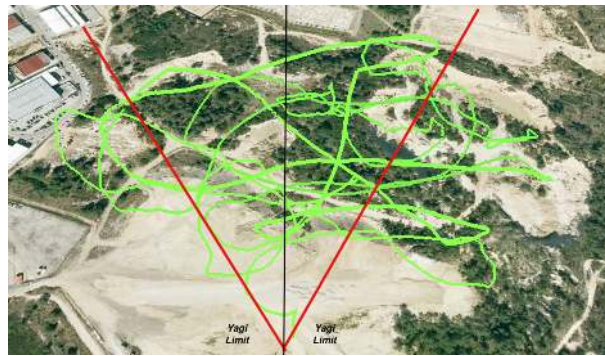
Figure 7.2: Line of travel for the short range Flight.

The flight path is shown in Fig. 7.2. Figures 7.3 and 7.4 show the variation of the RSSI as the distance home and roll change over time. Before evaluating the level of RSSI, it is important to say that the Yagi antenna was never moved during the whole flight in order to evaluate the directivity of the antenna; it was placed always facing NorthEast with an output power of 500 mW.
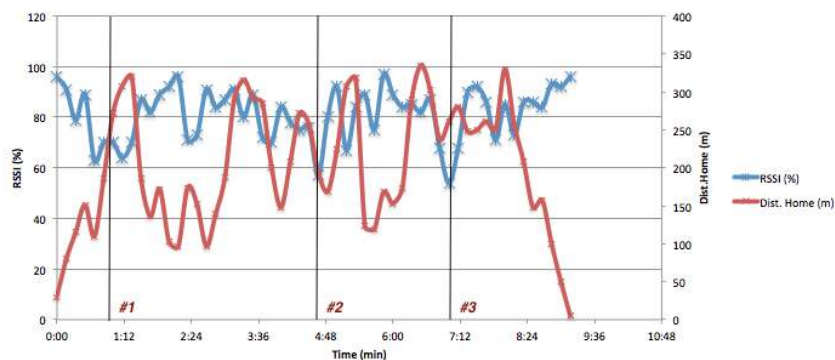
Figure 7.3: RSSI versus distance home.

Regarding the influence of the distance home for short ranges, it is seen in Fig. 7.3 that the point of maximum distance shows a level of RSSI of 82%. The same figure shows that for short ranges the RSSI is not greatly influenced by distance. It is also shown a lack of tendency for continuity meaning

the RSSI has inconstant readings and can only be seen as a reference since it can vary from 60 to 90% in short periods of time. According to 3DR [70], it was found that the reason why this happened was maybe due to the fact that while in the air, measuring signal strength becomes a difficult task because of radio and magnetic interference from external factors, such as wireless networks, television antennas, etc. Antennas on receivers catch all of this different radio signals all the time. Having other sources of the same frequency will affect measures.

Figure 7.2 shows three distinct pin points. These pins represent periods where the UAV went out of the Yagi's directivity limit (which is 30°) and, with the help of Fig.7.3, it is possible to see that even in a short range the directivity of the Yagi is important. In pin 1, the RSSI is at an average of 70% at a distance of 300 m, in pin 2 the RSSI is stronger that in 1 but it is still noticeable its decrease to an average of 75%. The same goes for pin 3 with an average of 65%.

As for the influence of banking manoeuvres on the RSSI, shown in Fig.7.4, it is seen that the diversity capability of the TSLRS Rx is properly effective since, for example, at minute 1:40 (#1) the UAV is manoeuvring with a roll of -39° and the RSSI reads 85%.
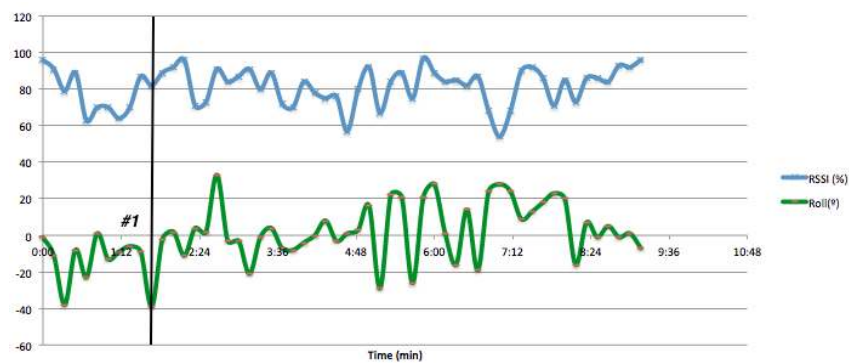
Figure 7.4: RSSI versus the Roll of a certain manoeuvre.

7.1.2 Video Link Quality

The same flight from Subsection 7.2.1 is analysed but now from the point of view of video quality. Just as was done with the Yagi, the helical was not moved during the whole flight, with Fig.7.5 showing the directivity limits of the helical antenna (which is 60°). It is noticeable that the UAV did not get outside those limits.

Despite being inside these limits there are still some glitches and images distortions. It was found that the image would distort mostly around the telemetry data. As in Section 6.2, this was found to be due to the coding behind the MinimOSD since the coupling of the video transmission with the MinimOSD degrades the video. Fig. 7.7 exemplify this issue.

As for glitches due to banking, this was found to have two sides: the manoeuvre with maximum bank angle (-39° roll), seen in Fig.7.6, mentioned in Section 7.2.1 does not show any kind of glitch or distortion. However, lingered banking manoeuvres would somehow distort the image. This again can be

69

Figure 7.5: Overall flight data for a short range flight.

Figure 7.6: Banking of -39° with no image distortion.

attributed to the coding of the MinimOSD since the same happened in Section 6.2 where fast movements were tested with and without the MinimOSD.

(a)   (b)

Figure 7.7: Distortion due to transmission through the MinimOSD.

Finally, on another flight it was tested the importance of the video antenna direction, since it had such a wide opening (60°) when compared with the Yagi. The UAV was flown nearly parallel to the GCS (it was doing almost 180°) with the helical direction and the result was the video was very disturbed, see Fig. 7.8.

Regarding the use of the camera gimbal, it can be said that it has a great potential depending on
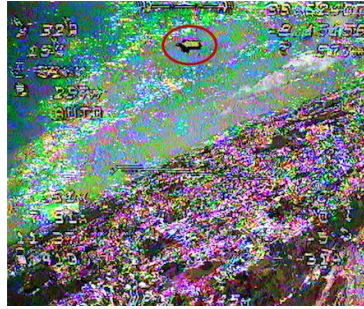
Figure 7.8: UAV flown in the direction of the GCS doing 180° with the Heliaxial orientation.

how it is used. During flight, two modes were experimented: one that used the gimbal to stabilise the image and another that enabled the gimbal to be used only in manual mode. The gimbal stabilisation test did not retrieve positive results. Despite working properly it just turned the flight confusing to the pilot (through the screen). Figure 7.9 a) exemplifies how a simple pitch manoeuvre would totally block the view making it dangerous. The manual mode of the camera gimbal, on the other hand, turned out to be a useful feature. This way, the pilot was able to recognise the field and its current position with pitching down. Fig. 7.9 b) shows an example of that.

(a) UAV climbing with the stabilise enabled.

(b) UAV recognising the field with manual gimbal.

Figure 7.9: Camera gimbal operation modes.

In conclusion, the camera gimbal has great potential when used manually. The stabilisation will block the view for the pilot but manually it enables him to perform recognition.

7.1.3 Overall Flight Quality

In this short range flight the UAV went up to a maximum distance of 396 m and travelled a total of 4829 m spending only 1451 mAh (35%) of the battery. The UAV was considered a stable platform for a longer range. Since it was proven in Chapter 6 that the UAV could handle, both in video and control, a flight with a maximum range of 8 km, a flight with 2 km of maximum range was planned and its results are presented and analysed in the Section 7.2.

71

7.2   Longer Range Flight Test

The chosen date for this flight test was when weather conditions were, once again, favourable as specified in Table 7.2.

Condition	Value
Wind Velocity (km/h)	9
Gust (km/h)	12
Direction	East
Temperature (^{o}C)	12-18
Humidity (%)	20

Table 7.2: Weather conditions during the longer range flight test.

The flight test was again conducted at *Pista de Aeromodelismo de Corroios* which provided a safe place to do all the necessary pre-flight (and flight) checks before attempting a new range mark. The goal of this test was to evaluate the performance of both the RC and video links while going further and further from the ground control station. The whole flight was done in manual mode.

7.2.1   RC Link Quality

This flight test was performed, solely, in manual mode since the interaction between the RC Tx and Rx is one of the two subjects of evaluation.

For safety reasons, the Yagi antenna was manually oriented so that the levels of RSSI were as high as possible. The farther the UAV was, the more difficult it was to orient the Yagi (the output power of the TSLRS was always at 500 mW). The whole ground station was powered by a car battery since all its equipment works at 12 V and and the battery can be, constantly, recharging. The sense of orientation of the pilot played a major role in this flight.

The values of RSSI were retrieved in order to evaluate its variations within a maximum range of 2200 m. The flight path can be seen in Fig.7.10.

Figure 7.10: Flight path of the 2.2 km flight test.

Regarding the relation between the distance home and the RSSI, it is seen from Fig.7.11 that when the distance increases, the RSSI decreases as expected. The peak of maximum distance retrieves a RSSI of 79%.
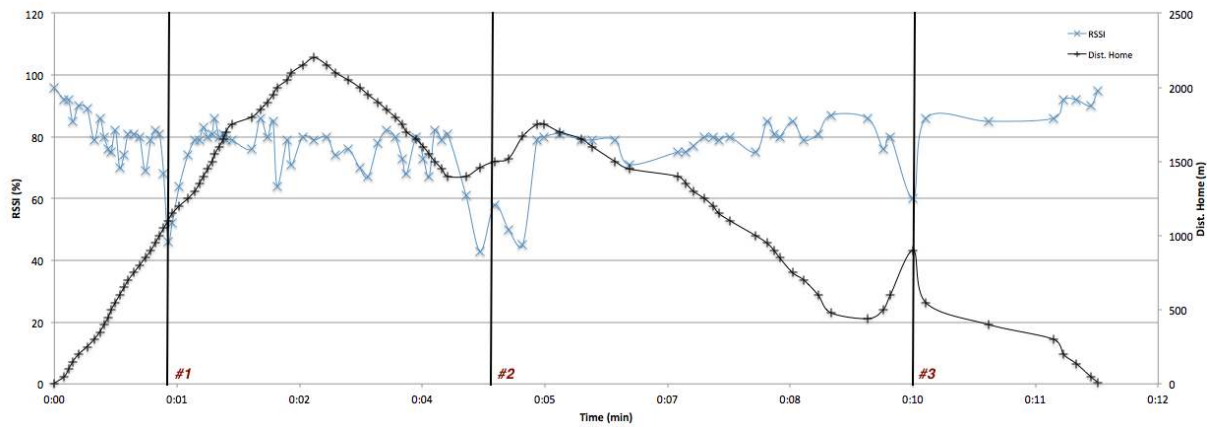
Figure 7.11: Overall flight data for a short range flight.

Comparing this result with the ground tests from Fig.7.3, it can be said that ground effects can greatly influence the link since on the ground, at 2 km distance, the retrieved RSSI was 60% and in the air the RSSI retrieves 79%.

In Fig. 7.11, there are three marked situations where the RSSI drops below 50%. On the first pinpoint (#1), it is seen that, the RSSI drop is very short. This fast rise is explained by the fact that the UAV was still in line of sight and the Yagi was easily reoriented. The second fall was already on the way home and the UAV was not in line of sight. For this reason, the drop lasted thirty seconds. When the Yagi and UAV were realigned, the RSSI retrieved 79%. From the second pinpoint (#2) to the third (#3), the Yagi is not reoriented. However, the pilot changes the course of the UAV so that the influence of the directivity can be evaluated for a longer range then in Section 7.1.1. As it can be seen from Fig.7.11, minute 10 is where the directivity is greatly noticed: the UAV is 1 km away and 42° 'rotated' from the Yagi orientation (in theory 30° would be the limit) and the RSSI, suddenly, drops to 60%. The Yagi is reoriented and as soon as this happens the link raises its strength to 86%.

In conclusion, although the RSSI is influenced by propagation loss, the parameter that most affected this flight was the directivity of the antenna (the same happened to the video link). Also, comparing the performance of this link with the performance on the ground it can be said that this system can top a range of, at least, 7 km.

7.2.2 Video Link Quality

As done for the short range flight, the 2200 m flight is also analysed in terms of video issues (and quality). Just as it was done with the Yagi, not to take any risks, the Helical antenna was hand-oriented so that those issues could be minimized.

The flight path is shown in Fig.7.10. In the same figure are marks that represent issues from the video link that were found to be noteworthy.

(a) UAS performing a banking manoeuver.　　(b) Obstructed heliaxial antenna.

Figure 7.12: First pinpoint (#1) remarks.

In the first pinpoint (#1), two situations were tested: the polarization loss issue, seen in Fig.7.12(a), and obstruction, in Fig. 7.12(b). The polarization loss was tested by making a banking manoeuvre with a roll angle of $53°$ (from the same figure the sky can be considered as very gray, this is due to the direct exposure of the camera lens to sun light) and the result was positive for the circularly polarized configuration since there are no interferences of any kind.

As for the obstruction issue, one person stood right in front of the helical antenna and the conclusions from Section 6.2 (of this fact) are once again confirmed. Although this is the less affected configuration, it can be seen from Fig. 7.12(b) that obstruction can greatly affect the video link. It is noteworthy that the obstruction test was done only 26 m away from the ground station.

(a) UAS at 69m.　　　　　　(b) UAS at 140m.

Figure 7.13: UAV gaining altitude and with the Helical pointed directly towards it (#2).

On the second pinpoint (#2) the helical antenna was oriented towards the UAV and the image became clearer when compared with the one from pin #1 (Fig.7.12(a)), as can be seen in Fig.7.13(b).Also, at this point, the UAV is 100 m higher then in pin (#1) which, also, means the ground effects are less influential on the video quality.

The third pinpoint (#3) is noteworthy because at this point, the antenna was readjusted and when comparing Fig.7.14(a) with Fig.7.14(b) from pinpoint #2, it is clear that an antenna repositioning makes all the difference.

On the forth pinpoint (#4), the pilot has to do a terrain recognition (making the speedway the stadium its reference points), as seen in Fig.7.14(b) so that the ground station antennas could be reoriented

(a) Effect of reorienting the Helical antenna towards the UAV (#3).

(b) Making use of the camera gimbal to do a terrain recognition (#4).

(c) Video loss at 2.03 km from the GCS (#5).

(d) Image recover after reorienting Helical antenna (#7).

(e) UAV performing a 61° manoeuvre with any image conflict (#8).

(f) Signal loss, at short range, due to antenna orientation (#9).

Figure 7.14: Remarks from pinpoints #3 to #9.

towards the UAV.

Regarding pinpoint #5, the UAV is now 2.03 km away from the Ground Station and the video starts to get weak, flickering and smearing appear, as seen in Fig. 7.14(c). The pilot recognises the situation and moves 100 m North (towards pinpoint #6) and that is where the video link improves significantly, as seen in Fig.7.14(d).

Pinpoint #7 is where the flight range achieves its maximum value of 2193 m. The video link is now getting smeared and the pilot decides to return home because moving the antenna might mean losing the link entirely. This does not mean the maximum range of the video system is 2 km, it just means that it gets harder to reposition the antenna without knowing the exact direction the UAV. It is easy to come to the conclusion that orienting the antennas manually is not advisable for long range flights. The use of an antenna tracker is definitely more advisable.

Pinpoint #8 is yet another confirmation that the circular polarization was a good choice, as seen in Fig. 7.14(e). The UAV is, now, almost 1 km away, performing a banking manoeuvre of 61° and the video link is not affected by it.

In Pinpoint #9 shows a video link completely lost, as seen in Fig.7.14(f). However, since the UAV is already in line of sight, the antenna was easily readjusted. This point shows how relevant an antenna tracker can be.

7.2.3 Overall Flight Quality

Pinpoint #10 marks the landing of the UAV and end of the flight. The UAV travelled a total of 8.7 km and it only spent 2425 out of a 3S LiPo battery with 4200 mAh capacity. The most limiting factor was not having the 3DR telemetry radio telling the pilot where the UAV was since it has a maximum range of 500 m with the current configuration. However, the obtained telemetry data retrieved from the OSD showed to be very reliable. Combining that with the use of the camera gimbal was enough to guide the pilot successfully.

The risk of losing the video and/or RC links in the middle of a flight is a threatening reality. Thus, the use of an antenna tracker is something to consider. The use of a different antenna (directional with higher gain) on the 3DR telemetry radio will give more range to the antenna tracker however, the radio can only emit at an output power of 100 mW.

Chapter 8

Final Considerations

A solution for Remote-person view (RPV) using commercial off-the-shelf (COTS) equipment is presented and analysed. For the success of this dissertation, mission objectives and RPV requirements are defined and explained.

Next, a RPV design is proposed and evaluated in a controlled environment and also through flight testing. The performance of this Unmanned Air Systems (UAS) is, then, used to evaluate the choices made and to propose a definite and better solution for long range UAS. The platform in question is composed by two main systems: the radio control and the video feed that together connect the UAV to the pilot.

The radio control link between the ground station and the UAV consists primarily of an up-link transmitting command from the pilot to the UAV. This transmission of commands is done on a radio frequency of 433 MHz and a permissible output power between 0.5 and 2 W allowing a sufficient bandwidth per channel to encode digital data, within the limits of the law, to travel long distances.

The video feed, on the other hand, makes use of a small video camera and an analogue video system on a radio frequency of 1.2 GHz and a permissible output power of 850 mW in order to fly by means of a live video down-link displayed on a portable monitor. This video system is, also, retrieving telemetry data through the flight controller and an on-screen display.

(a) RPV long range configuration. (b) RC long range configuration. (c) Ranges in controlled environment and in flight tests.
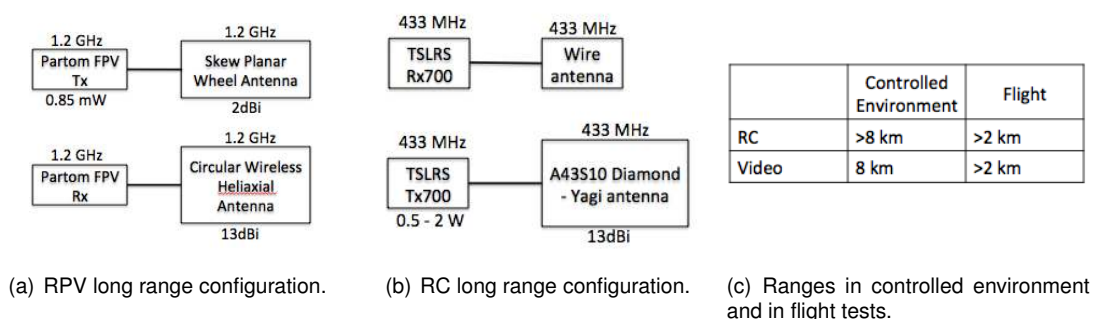
Figure 8.1: Final configuration for long range flights.

In both systems, directional antennas of high gain are used on the ground station to see that it is not necessary to spend to much energy in order to have a signal travelling long distances. After proposing

the overall COTS systems, several tests are conducted in order to do an estimate of the range and quality of the same.

In order to perform these tests, parameters that best characterize each system are proposed. For the characterization of the control system, a straight forward parameter is used: the RSSI (provided through an analogue pin of the RC receiver) is used to evaluate 2 different antenna configurations in a controlled environment.

As for video feed, since through research, it was concluded that retrieving the Signal to Noise Ratio (SNR) to have a unit of measure for the video range is not enough, the same is characterized using a subjective method called Mean Opinion Score (MOS) which relies on the opinion of viewers to evaluate the image quality in terms of: colours, contrast, borders, movement continuity, phenomena of flickering and smearing. Other three issues that often occur in video transmissions are considered: polarization loss, antenna pattern null and signal obstruction.

8.1 Achievements

The major achievements of the present work can be summarized as follows:

- Design and setup of a video system that enables long range flights, including the primary components such as a camera, camera gimbal, transmitter and receiver, on-screen display with telemetry data, ground display and antennas;

- Design and setup of a control system that enables long range flights, including the primary components such as remote controller, LRS transmitter and receiver and antennas;

- Radio Control range tests in a controlled environment such as: a) signal strength as a function of distance, b) antenna directivity;

- Video range testing in controlled environment such as: a) propagation loss, b) polarization loss, c) antenna pattern null and d) signal obstruction and e) antenna directivity;

- Implementation and validation of the purposed setup by means of analysis of quality and range in actual flight tests taking into account, in both systems, the importance of: a) distance, b) baking, c) signal obstruction, d) antenna directivity;

- Development of a platform capable of communicating at long distances that is not an end in itself but an open project that can be used for many purposes depending on the will of the project it is inserted in.

A final antenna configuration was reached and, 2 m above the ground, the video configuration, as seen in Fig. 8.1(a), showed a maximum range of 8 km while the RC configuration, as seen in Fig. 8.1(b), also 2 m above the ground, proved to be able to perform at least, 8 km. After gathering conclusions regarding the best antenna configurations for video and RC, the same was applied to a flight test in which its strengths and weaknesses were analysed.

A maximum flight range of 2.2 km was reached. Although the UAS seemed to handle a lot more than 2 km it was decided it was better for the UAS to return home because it was getting to hard to manually point the antennas towards the UAV as it got out of sight. Extrapolating, the UAS, with a 3S LiPo battery, on board can perform flights of 10 km distance and still have 25% of battery reserve which can is summarized in Table 8.1(c).

With that said, it was proved in this dissertation that the system is suitable for distances of, at least, 8 km and that range is limited by the fact that the ground station antennas are not directly pointed to the UAS as it gets harder to manually point them for distances that are out of the line of sight.

8.2 Future Work

There is, however, potential for enhancing the obtained results. The major concern during flight testing was the orientation of the ground station antennas towards the UAS. The use of an antenna tracker should be tested, analysed and implemented the same way as the other systems were in this dissertation.

In order to break barriers in terms of range and endurance, a structure with concerns in aerodynamic performance should be implemented and also the use of solar panels that no longer makes energy an issue. Also, the use of the flight controller's autopilot feature should be explored in a long range mission. When considering an UAS that not only can perform long distance flights but also flights of long endurance the pros and cons of using directional antennas have to be measured: they allow the UAV to travel long distances but with narrow angles of directivity which limits its applications at long distances. To solve this issue, a long range antenna tracker has to be implemented.

Bibliography

[1] R. Austin. *UAS Design Development and Deployment*. Wiley, Wiltshire, United Kingdom, 2010.

[2] B. Brown. Will drones soon replace architects? `http://architizer.com/blog/will-drones-soon-replace-architects/`, June 2014. Accessed: 2014-10-13.

[3] Watch a drone visit college football to give coaches better perspective. Tchcrunch Website, Gregory Ferenstein. Accessed: 2015-04-1.

[4] José António Cerejo. PSP compra veículos aéreos não tripulados. Jornal O Publico, December 2013.

[5] T. Hong. Air Quality Plume Characterization and Tracking Using Small Unmanned Aircraft. 2011. University of California, San Diego.

[6] Jacopo Pasotti. Stillfly the newest weapon in the fight against illegal waste dumping. 2012.

[7] Amy Gahran CNN. Fighting fire with data, spacecraft, drones. CNN, July 2012.

[8] Rebecca Boyle. Introducing the matternet, a network of drones for deliveries in remote locations. popsci, August 2011.

[9] J.E. Nyquist. Applications of low-cost radio-controlled airplanes to environmental restoration at oak ridge national laboratory. In Proceedings of the 23rd Annual Association for Unmanned Vehicle Systems International Symposium and Exhibition Innovations for the Future, 1996.

[10] M. C. Quilter and V. J. Anderson. Low altitude large scale aerial photographs a tool for range and resource managers. *Rangelands*, 2000.

[11] Digital photos from solar airplane to improve coffee harvest. `http://www.nasa.gov/centers/ames/news/releases/2002/02_27AR.html/`. Accessed: 2014-10-22.

[12] S.T. Simpson, T. Stombaugh, L. Wells, and J. Jacob. Imaging techniques and applications for uav in agriculture. *International Journal of Agricultural and Biological Engineering*, 6(031105), 2003.

[13] P.J. Hardin and M.W. Jackson. An unmanned aerial vehicle for rangeland photography. *Rangeland Ecology and Management*, 58(4), 2005.

[14] V. Espinar and D. Wiese. An extreme makeover: scientists upgrade a toy plane with robotic technologies. *GPS World*, pages 20–27, 2005.

[15] P. Clegg, L. Bruciatelli, F. Domingos, R.R. Jones, M. De Donatis, and R.W. Wilson. Digital geological mapping with tablet pc and pda: A comparison. *Computers and Geosciences*, 32(10):1682–1698, 2006.

[16] B.R. Dingus. The use of unmanned aerial vehicles for aerobiological sampling. M.s. thesis, Virginia Polytechnic Institute and State University, 2007.

[17] A. C. Marta and P. V. Gamboa. Long endurance electric UAV for civilian surveillance missions. In 29th *Congress of the International Council of the Aeronautical Sciences, St. Petersburg*, 2014.

[18] Piotr Rudol. *Increasing autonomy of unmanned aircraft systems through the use of imaging sensors*. Ph.d thesis, Linköpings universitet, 2011.

[19] Autoridade Nacional de Comunicações. Quadro nacional de atribuição de frequências. Accessed: 2014-11-27.

[20] Autoridade Nacional de Aviação Civil. Seminário sobre regulamentação de RPAS. February 2015.

[21] D. Grini. Rf basics, rf for non-rf engineers. MSP430 Advanced Technical Conference, 2006.

[22] L. Barclay. *Propagation of Radiowaves*. Electronic Waves Series 502, 2008. ISBN-13: 978-0852961025.

[23] D. M. Pozar. *Microwave Engineering*. John Wiley and Sons Inc, 2012.

[24] If the lower the frequency, the longer the range why not building, for example, a 72mhz lrs system. Information retrieved from private e-mail conversation with Patrick Mikkelsen and Steven Friberg, . Accessed: 2015-02-24.

[25] Harmonics and frequency planning technical breakdown of tslrs ezuhf dragonlink. `https://www.youtube.com/watch?v=RFC9PDTjJ4E`. Accessed: 2014-02-26.

[26] Sba responds to scherrer uhf. `https://www.youtube.com/watch?v=Q4V20e7PCg0`. Accessed: 2014-02-26.

[27] Scherrer UHF Long Range System. Manual for tx700. November 2013.

[28] H. Chao, Y. Luo, L. Di, and Y. Chen. Fractional order flight control of a small fixed-wing uav controller design and simulation study. In *Proceedings of the 2009 ASME International Design Engineering Technical Conference Computers and Information in Engineering*, 2009.

[29] Duarte Lopes Figueiredo. Autopilot and ground control station for uav. M.s. thesis, Instituto Superior Técnico, October 2014.

[30] H. Chao, Y. Cao, and Y. Chen. Autopilot for small unmanned aerial vehicles: A survey. *International Journal of Control Automation and Systems*, pages 3144–3149, August 2007. doi:10.1007/s12555-010-0105-z.

[31] *APM 2.6 Autopilot User Manual*. 3DRobotics, March 2013.

[32] *Pixhawk Autopilot User Manual*. 3DRobotics, March 2014.

[33] *On Screen Display Autopilot for Model Airplanes User Manual*. RangeVideo, August 2012.

[34] C. A. Balanis. *Antenna Theory: Analysis and Design*. John Wiley and Sons Inc, 2010.

[35] Agostinho Fonseca. Apontamentos de ensaios em voo. Instituto Superior Técnico, Portugal, 2011.

[36] Antenna polarisation. `http://www.air-stream.org.au/technical-references/` `antenna-polarisation`. Accessed: 2015-01-05.

[37] Diamond Antenna. A430s10 base station yagi beam. January 2007.

[38] *UHF RC system, MCX wire antenna detailed datasheet*. Thomas Scherrer LRS, February 2011.

[39] Joshua Bardwell. About 802.11 signal and noise metrics. Document D100201, 2004.

[40] H. T. Friis. A note on a simple transmission formula. *I.R.E. and Waves and Electrons*, 1946.

[41] Carlos Fernandes. Estimar o alcance de uma ligação assumindo desimpedida utilizando a equaçã de friis. Instituto Superior Técnico 2014.

[42] *First Person View (FPV) Policy*. Model Aeronautical Association of Australia, August 2012.

[43] C. Ononiwug, O.J. Onojo, and N. Chukwuchekwa. Uav design for security monitoring. *International Journal of Emerging Technology & Research.*, II(2), March 2015.

[44] B. Kang, J. Kim, and H. Yang. Design of multi-standard ntsc/pal video encoder. *Current Applied Physics*, 4:37–42, 2004.

[45] R. Hain, C. J. K'ahler, and C. Tropea. Comparison of CCD, CMOS and intensified cameras. *Experiments in Fluids.*, 42(3), March 2007. doi 10.1007/s00348-006-0247-1.

[46] Kx-181 camera ccd camera. `http://electronicarc.com/catalogo/product_info.php?` `products_id=439&osCsid=a1680012e8e8b24100ce0e9750b3158e`. Accessed: 2014-10-13.

[47] 3DRobotics. Video/OSD kit. December 2013.

[48] *EzOSD Overview & Operating Instructions*. Immersion RC, April 2009.

[49] ElectronicaRC. Partom 850 mW 1.2 GHz video system datasheet. May 2014, .

[50] ElectronicaRC. Lawmate 1.2 GHz 1000 mW video system datasheet. May 2014, .

[51] ElectronicaRC. DJI Lightbridge - 2.4 GHz full HD digital video downlink. Aug 2014, .

[52] Circular wireless products page. `http://www.circular-wireless.com/en/products-page`. Accessed: 2014-11-6.

[53] Circular Wireless. Skew planar wheel. January 2007.

[54] Circular Wireless. Helical modo axial. January 2007.

[55] Fieldview 1010 tft high definition lcd monitor for fpv 1366x768 led backlight (10.1 inch). `http://electronicarc.com/catalogo/product_info.php?products_id=1195&osCsid=7c6b025c8274cec5164f7099c80b117e`, October 2013. Accessed: 2014-10-13.

[56] Hobbyking website for model testbed. `http://www.hobbyking.com`. Accessed: 2014-10-22.

[57] Q. Huynh-Thu and M. Ghanbari. Scope of validity of PSNR in image/video quality assessment. *Electronics Letters*, 22(13), 2012.

[58] Y. A. Al-Najjar and D. Chen Soong. Comparison of image quality assessment: PSNR, HVS, SSIM, UIQI. *International Journal of Scientific and Engineering Research*, 3(8), 2012.

[59] National Instruments. Peak signal-to-noise ratio as an image quality metric. National Instruments, 2013.

[60] Z. Wang. Why is image quality assessment so difficult. *Acoustics, Speech and Signal Processing (ICASSP)*, IV:3313 – 3316, 2002.

[61] A. Watson, J. Hu, and J. McGowan III. Dvq: A digital video quality metric based on human vision. *Journal of Electronic Imaging*, pages 20–29, 2001.

[62] Telecommunication Standartization Sector of ITU. Subjective video quality assessment methods for multimedia applications. International Telecommunication Union, 2008.

[63] Ardupilot APM and PX4 Configuration for Plane. `http://plane.ardupilot.com/wiki/arduplane-setup/first-time-apm-setup/`. Accessed: 2015-04-1.

[64] A3DRobotics UAV Technology. Apm 2.6 for external magnetometer. December 2013.

[65] Minimosd-extra support website. `https://code.google.com/p/minimosd-extra/`. Accessed: 2014-02-19.

[66] why the skew planar antenna is better than a standard whip antenna? Information retrieved from private e-mail conversation with Juan (Sircana). Accessed: 2015-02-24.

[67] Telecommunication Standartization Sector of ITU. Subjective video quality assessment methods for multimedia. *Recommendation ITU-T P.910*, 2009.

[68] Windguru. `http://http://www.windguru.cz`. Accessed: 2015-04-16.

[69] Accuweather. `http://www.accuweather.com/pt/pt/portugal-weather`. Accessed: 2015-04-16.

[70] The rssi is very inconstant: while cruising or manoeuvreing the rssi can vary from 93 to 70. Information retrieved from private e-mail conversation with Aram Robledo (3DR Tech Support Engineer), . Accessed: 2015-04-24.

[71] Alexander Greve's Do It Yourself Antenna Tracker. http://www.rcgroups.com/ forums/showthread.php?t=1337608. Accessed: 2015-05-10.

[72] B. Etkin. *Dynamics of Flight: Stability and Control*. John Wiley & Sons, Wiltshire, United Kingdom, 1995.

[73] APC Propellers. 9x6 performance datasheet. December 2014.

[74] T. C. Corke. *Design of Aircraft*. Pearson Education, 2003. ISBN 13: 978-0130892348.

[75] Maximum lift coefficient of the skywalker airframe. `http://www.rcgroups.com/forums/showthread.php?t=1223595&page=525`. Accessed: 2014-01-30.

Appendix A

Design of an Antenna Tracker

Antenna Trackers are systems that track the UAV's location, and use this information to correctly align a direction antenna. From ground and flight testing it was found that in long distances it was hard to point the antenna to where the UAV was exactly and for this reason, the design of an antenna tracker using COTS products is addressed in this appendix. This approach significantly improves the range over which signals can be both sent and received from the ground station.

A.1   Problem Statement

Designing an antenna tracker for the purpose of this dissertation has two different ramifications: 1) using the equipment already available and 2) designing it for long range.

With the available equipment there are two possible approaches:

1. Using the Telemetry 3DR-radio to provide the tracker the GPS coordinates to determine Azimuth (heading) and direct the antennas; Item Using a system that instead, uses raw signal strength (RSSI).

The first uses the 3DR-radio which is a transceiver with an output power of 100 mW which was not designed for long range flights. It would be possible to adjust that coupling it with a high gain and very directional antenna like a parabolic dish.

The main problem of using the 3DR-transceiver is that the ground station would have three antennas with two of then working in the 433 MHz frequency band which is not advisable due to interference reasons

The second design is retrieved from a post of Alexander Greve in RCGroups [71] that designed an antenna tracker which, instead of using GPS coordinates to determine azimuth (heading) to direct the antennas beam, uses raw signal strength (RSSI). This way there will be no need of using the telemetry radio that had a limited output power of 100 mW.

The design from Alexander Greve was chosen because this antenna tracker, working properly will have the same range as the video system (and not the range of the the telemetry system adaptation).

A.2 Long Range Design

All the needed parts are commonly available which is a plus because they can be bought online or in a local store. The list of parts is summarized in Table A.1:

1 - PCB board (5x7 cm; 2.5 cm hole spacing);   1 – Resistor (270 KΩ);
1 - voltage regulator (uA 7805);   2 – Resistors (22 KΩ);
1 – voltage comparator (LM393);   6 – Resistors (15 KΩ);
1 - Operational Amplifier (OpAmp) (LM358);   2 – Resistor (2 KΩ);
2 – 555 timer (NE555N or NE556N);   1 – resistor (390 Ω);
2 - electrolytic capacitor (1μF);   2 – Diode (N4148);
1 - Capacitor (4.7 μF);   1 – Heatsink (TO-220);
1 – Capacitor (1 μF);   1 – Standard size servo;
2 – Potentiometers (100 KΩ);   3 - Video Rx;
1 – Potentiometer (1 Mega Ω);   3 - directional antennas.

Table A.1: List of parts needed to build an antenna tracker [71].

Figure A.1 shows the tracker control board schematics.
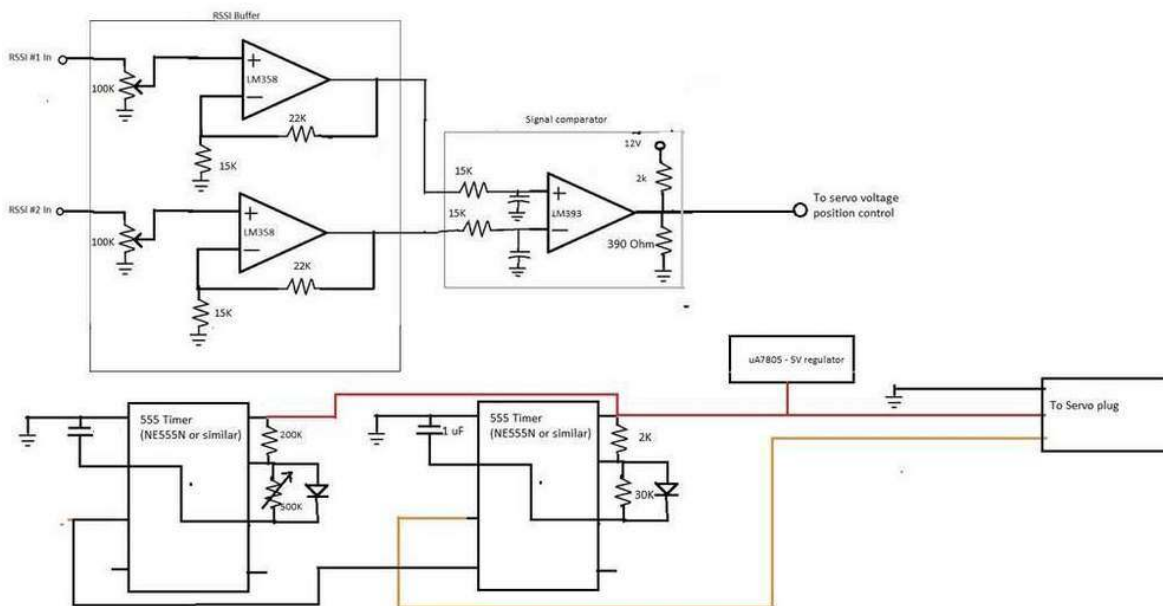
Figure A.1: Tracker board schematics [71].

The RSSI pin will be used to determine the position of the UAV, comparing the voltages between the two Rx and the third unit will be the receiving module. Locating the RSSI pins in the receiver is done by checking voltages on each pin, turn on and off the radio Tx and see which pin changes voltage.

The RSSI buffer reduces the impedance of the RSSI and disconnect it from the circuit when it changes state using the Operational Amplifier LM358.

The signal comparator does the actual selection of the signals. Its inputs are the two RSSI voltages and it outputs a 5 V or 0 V signal.This tells the channel selector which unit to select. Once selected, the output is then buffered through an adjustable Schmitt trigger circuit (by adding a single potentiometer to

the LM393) to keep it from switching unnecessarily fast between the two units.

Fig.A.2 shows the printed circuit board layout of the antenna tracker.
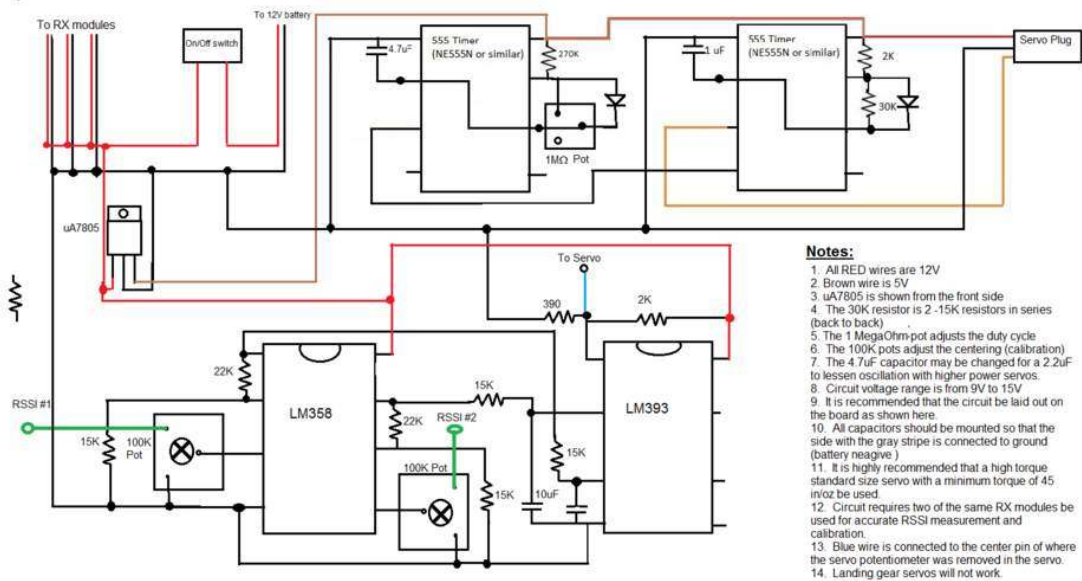
Figure A.2: Antenna tracker layout [71].

Figure A.3 shows Alexander Greve's own prototype.

(a) Up view.

(b) Front view.

Figure A.3: Alexander Greve's own prototype [71].

Appendix B

Airframe and Engine Testbed Selection

B.1　Airframe Testbed Selection

There are three types of fixed-wing airframes: the traditional, sports-glider (or pusher) and flying wing. Their pros and cons are shown below:

A brief web research is enough to understand that there are lots of options available: long-endurance airframes have many reviews on what to look for and what not to get. The second search was focused on what other people have done and what do they recommend. Out of many, 5 models, in which all of them are fixed-wing airframes, stood out and were taken into account. Their specifications are gathered in Table B.1.

	EPP-FPV	Skywalker X-8	Skywalker2013	Skywalker 2014	Skywarrior
Fuselage length (mm)	1150	NA	1180	1300	1400
Wing Span (mm)	1800	2120	1900	1800	2030
Airframe Weight (g)	1000	3500	1300	1300	1800
Price	54	127	85	110	170

Table B.1: Main specification of the selected airframes.

The EPP-FPV, for being the cheapest airframe and lightest (weighting only 1 kg with the 2013 being the second most light with 1.8 kg), is tempting but it lacks space for storing all the necessary electronics which means that they would have to be placed outside the airframe translating in aerodynamic drag.

The Skywalker from 2013 is the one with the most reviews and recommendations. It has many videos available verifying its reliability and is the second most light. For being around for quite a while its price is very reasonable.

The Skywalker from 2014 was found in a local shop which would mean less time spent ordering and ease the buying. On the other hand the 2013 Skywalker has been around for some time and for that is much more less expensive and there are lots of flight test video of the internet showing that it is a capable and reliable airframe.

The Skywarrior lacks in detailed description, also there are no flight test video available and it is priced at 165 . €

On the other hand, the flying wing X-8 seems to be a good approach due to its interior volume for placing all the electronics. Also, it is made of EPP too, which makes it as hard to brake as all the others. It also, received good reviews by the community.

The 2013 Skywalker is the airframe with better potential and will be the one used. Although they share similar qualities but it is best to buy an airframe that has shown good results from previous users and therefore has been around for a while. Also a light airframe will theoretically allow better results.

B.1.1 Weight Distribution

An aircraft can perform a steady flight if the resultants of the external forces and moments about the mass center both vanish, which implies the pitching moment to be zero. If an aircraft is longitudinally stable, a small increase in angle of attack will cause the pitching moment on the aircraft to change so that the angle of attack, α decreases. Similarly, a small decrease in angle of attack will cause the pitching moment to change so that the angle of attack increases. A non-zero pitching moment, C_m will cause a rotational acceleration in the direction of the unbalanced moment. The static stability is determined by the sign and magnitude of the slope $\frac{\partial C_m}{\partial \alpha}$. It can,then, be said that C_{m_0} must be positive and $\frac{\partial C_m}{\partial \alpha}$ negative if the airplane is to be in a condition of stable equilibrium [72].

It has been found both experimentally and theoretically [72] that, if the aerodynamic force is applied at %25 of the chord from the leading edge of a rectangular wing, the magnitude of the aerodynamic moment remains nearly constant even when the angle of attack changes. This location is called aerodynamic center (AC). To calculate the mean aerodynamic center of a tapered wing, equation B.1 may be used:

$$MAC = c_{root} * 2/3 * \frac{1 + \lambda + \lambda^2}{1 + \lambda},$$
(B.1)

where λ is the wing's taper ratio, $\frac{C_{tip}}{C_{root}}$, c_{root} the root chord and c_{tip} the tip chord . The center of gravity (CG) location range is usually between 28% and 33% ahead of the aircraft neutral point: this is called the static margin which should be between 5% and 15% ahead of the aircraft neutral point. The simplest way for calculating the neutral point is by using the areas of the two horizontal lifting surfaces as in Eq. B.2:

$$D = L * \frac{A_{Stab}}{A_{Wing} + A_{Stab}}$$
(B.2)

where D is the distance between the neutral point and the main wing aerodynamic center and L the distance between the two aerodynamic centers, A_{Stab} the area of the stabiliser, A_{Wing} the wing area.

For aircrafts with different aspect ratios in the two lifting surfaces a more accurate result can be obtained by the use of the tail volume ratio as in Eq. B.3 [72]:

$$D = \sqrt[4]{AR}0.25\frac{A_{Stabnet}}{A_{Winggross}}\frac{L}{MAC_{wing}} \tag{B.3}$$

The operating handbook of every airplane specifies the range over which the CG is allowed to move. Inside this range, the airplane is considered to be inherently stable, which is to say that it will self-correct longitudinal (pitch) disturbances without pilot input. However, in the Skywalker manual there is no indication of this margin and so an estimate for the position of the center of gravity will have to be made.

Aircraft Center of Gravity Calculation	
Wing Root Chord (m)	0.23
Wing Tip Chord (m)	0.21
Wing Sweep Distance (m)	0.02
Wing Half Span (m)	0.9
Stabiliser Root Chord (m)	0.17
Stabiliser Tip Chord (m)	0.11
Stabiliser Sweep Distance (m)	0.06
Stabiliser Half Span (m)	0.3
Distance between Leading Edges (m)	0.74
Stabiliser Type	T-tail
Static Margin	10%
Mean Aerodynamic Chord (m)	0.22
Sweep Distance at MAC (m)	0.01
From Root Chord to MAC (m)	0.44
Wing Area (m^2)	0.3944
Stab Area (m^2)	0.1
Aspect Ratio	8.96
Tail Volume ratio	0.71
From Wing Root Leading Edge to AC (m)	0.06
From Wing Root Leading Edge to CG (m)	0.11
From Wing Root Leading Edge to NP (m)	0.14

Table B.2: Skywalker data for the calculation of the center of gravity.

In cruise condition most of the lift force is generated by the wings, with ideally only a small amount generated by the fuselage and tail. The longitudinal static stability may be analysed by considering the aircraft in equilibrium under wing lift, tail force and weight. The moment equilibrium condition is called trim and is the aircraft condition of concern.

For an aircraft to be stable in pitch, its center of gravity (CG) must be forward of the Neutral Point (NP) by a safety factor called static margin, which is a percentage of the mean aerodynamic center (MAC). Table B.2 provides all the characteristics that allow an estimation. With this aircraft data and recurring to [72] it is possible to estimate the position of the ideal center of gravity.

The mean aerodynamic chord (MAC) was estimated to be 0.22 m located at 0.44 m from the wing root and the sweep distance at the MAC 0.01 m. Thus, the aerodynamic center is estimated to be at

25% of the root chord, the neutral point at 60% and the center of gravity at 48%. This is the reason why the batteries (the heaviest elements of the whole lot) will placed as far back as possible which coincides with the 48% of the wing root chord. The batteries will be placed below the canopy so the overall centre of gravity stays approximately at 50% of the wing root chord.

B.2   Electric Motor and Propeller Testbed Selection

B.2.1   Propeller

The Skywalker has the support for the motor on its back and so, the propeller size is limited by the distance between the engine support and the airframe tail. The airframe only allows a maximum diameter of 0.22 m for the propeller. Because of this, the chosen propeller was a 9x6 APC. where the 9 stands for 9 inches diameter (0,22 m) and the 6 for the pitch size as seen in Fig. B.1.
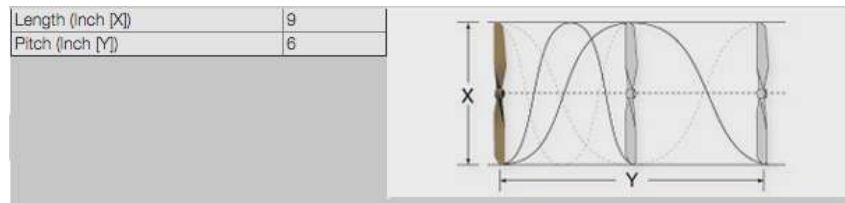
Figure B.1: 9x6 Propeller characteristics [56].

B.2.2   Electric Motor

In order to find a combination of electric motor and propeller that matches this UAV, empirical data is used as basis, supplemented by propeller data [73]. The parameters that will define if the motor is suitable for the aircraft are thrust (T), shaft horsepower (P) and engine and propeller efficiencies.

The first assumption is that the climb stage is the one that requires more power and more thrust. Assuming, also, that the climb will be at a constant rate (dV/dh=0, where V is velocity and h is altitude), the rate of climb becomes [74]:

$$\frac{dh}{dt} = V_{climb}\sin(\gamma) = V_{climb}\frac{T-D}{W} \tag{B.4}$$

where T stands for thrust, D for drag, W for weight and γ for the climb angle. And so, the required thrust for climbing can be calculated as

$$T = W\sin(\gamma) + D \tag{B.5}$$

For subsonic climb, the total drag is the sum of the base drag with the drag coefficient, C_{D_0} and the lift-induced drag. Therefore [74],

$$D = qSC_{D_0} + qSC_L^2/(\pi ARe) \tag{B.6}$$

where q stands for air dynamic pressure, S for platform area, AR for Aspect Ratio and e for wing efficiency factor (as in [74] assumed 0.8, for simplicity). Finally, an equation for the required thrust for climb is obtained in Eq. B.7:

$$T = W \sin(\gamma) + qSC_{D_0} + \frac{W^2}{q\pi AReS} \tag{B.7}$$

and also for the required Power in Eq.B.8 [74]:

$$P = T_{climb}V_{climb} \tag{B.8}$$

Table B.3 shows the parameters that, as of this moment, are known:

Spec	Value
Weight (N)	20
AR	8.96
S (m^2)	0.3944
ρ (kg/m^3)	1.225
S (m^2)	0.3944
γ (deg)	20

Table B.3: Measured specifications from the Skywalker Airframe.

Thus, it is necessary to estimate the climb velocity V_{climb} and the base drag coefficient, C_{D_0}.

Climb Velocity

From [74], V_{climb} is the velocity that is appropriate to the climb conditions. $V_{climb} = V_{takeoff}$ can be the representative velocity for the take-off climb. The velocity required for take-off is defined as a function of the stall velocity (V_{stall}) [74]:

$$V_{TO} = 1.2V_s = 1.2\sqrt{\frac{W}{S}\frac{2}{\rho C_{L_{max}}}} \tag{B.9}$$

where $C_{L_{max}}$ is the lift coefficient for maximum lift-to-drag ratio which is related to the maximum range. The value for $C_{L_{max}}$ was obtained empirically from pilots that suggested [75] an estimate of 1.72 which translated in a value for the stall speed of 8 m/s and a climb velocity of 10 m/s.

Base Drag Coefficient, C_{D_0}

To calculate the base drag coefficient the whole aircraft was approximated to a wing using turbulent flat plate studies. The base drag coefficient is given, in [74], as a function of the friction coefficient, C_f, the form factor, F, Wet Area-Area ratio, $\frac{S_{wet}}{S}$ and the interference factor, Q, as shown in B.10

$$C_{D_0} = CfFQ\frac{S_{wet}}{S} \tag{B.10}$$

where each parameter is estimated through B.11, B.12, B.13, respectively, and Q is approximately 1 for the high-wing configuration of the Skywalker (Table 4.2, p. 75, [74]).

$$C_f = \frac{0.455}{(log_{10}Re_x)^2.58} = 0.0068 \tag{B.11}$$

where Re_x is the Reynolds number and where the flow was considered solely turbulent in order to

estimate the worst case scenario of drag

$$F = [1 + \frac{0.6}{(x/c)_{max}}(t/c) + 100(t/c)^4][1.34M^0.18(cos(\Delta_{t/c_{max}}))^0.28] \tag{B.12}$$

where $(x/c)_{max}$ is the chord-wise location of the maximum thickness point of the airfoil section, t/c and $\Delta_{t/c_{max}}$ the sweep angle of the maximum thickness line [74].

$$\frac{S_{wet}}{S} = 1.977 + 0.52\frac{t}{c_{max}} \tag{B.13}$$

where Table B.4 shows the input parameters obtained from, actually, measuring the airframe and the output parameters that allows an estimation for the base drag coefficient:

Aerodynamic Specs.	
V_{climb}	10.2
c (m)	0.22
v	1.77 10^{-5}
Rex	1.267 10^5
C_f	0.0068
x/c	0.4
t/cmax	0.13
$\Delta_t/cmax$ (deg)	1.47
F	1.55
S_wet/S	2.044
C_{D_0}	0.022

Table B.4: Intermediate steps for calculation the Base Drag Coefficient.

Available Motors

Every required parameter is now computed and so, it is possible to estimate the required Thrust: T = 8.11 N and Power: P = 82.7 W. From the above estimate for the thrust and maximum power, an OS3810-1050 engine with specifications given in Table B.5 was chosen.

OS motor	3810-1050
Volts	12.6
kV(rpm/V)	1050
Weight (g)	102
ESC	50A
Battery	3S
Prop.	9x6E
Max. Thrust (kg)	1.3
Max.Power (W)	315

Table B.5: os3810specs

Although it was estimated the necessary output thrust of the propulsion system, when tested in the field, it did not seem to provide enough thrust since it turned out to be a day with some gusts (although it allowed for minimum consumption in cruise a gust might become a problem). This was done by holding the UAV by its wings, as in Fig.B.2(a), and giving it maximum thrust.

Having bought the engine the size of the propeller limited by its diameter there was the option of raising the motor axis by building a support. This would allow the use of blades with bigger diameters.

The support was done using a CNC machine (automation of machine tools that are operated by precisely programmed commands) and a light composite material. Fig.B.2(b) shows the final result.

(a) Test for Thrust.

(b) Final Result for the support of the motor.

Figure B.2: Radio-link system configurations.

With a new platform built 3 different propellers were tested and Table B.6 shows the thrust calculated for each one

	P(W)	I(A)	V	T(kg)
9x6	288	24	12	1.13
10x5	303	25	12	1.5
11x5.5	372	31	12	1.8

Table B.6: Experimental Data for each propeller using the same OS engine.

The 10x5 was chosen since it provided an increase of 25% in thrust with just an increase of 5% in input power.

Appendix C

Sub-systems Schematics
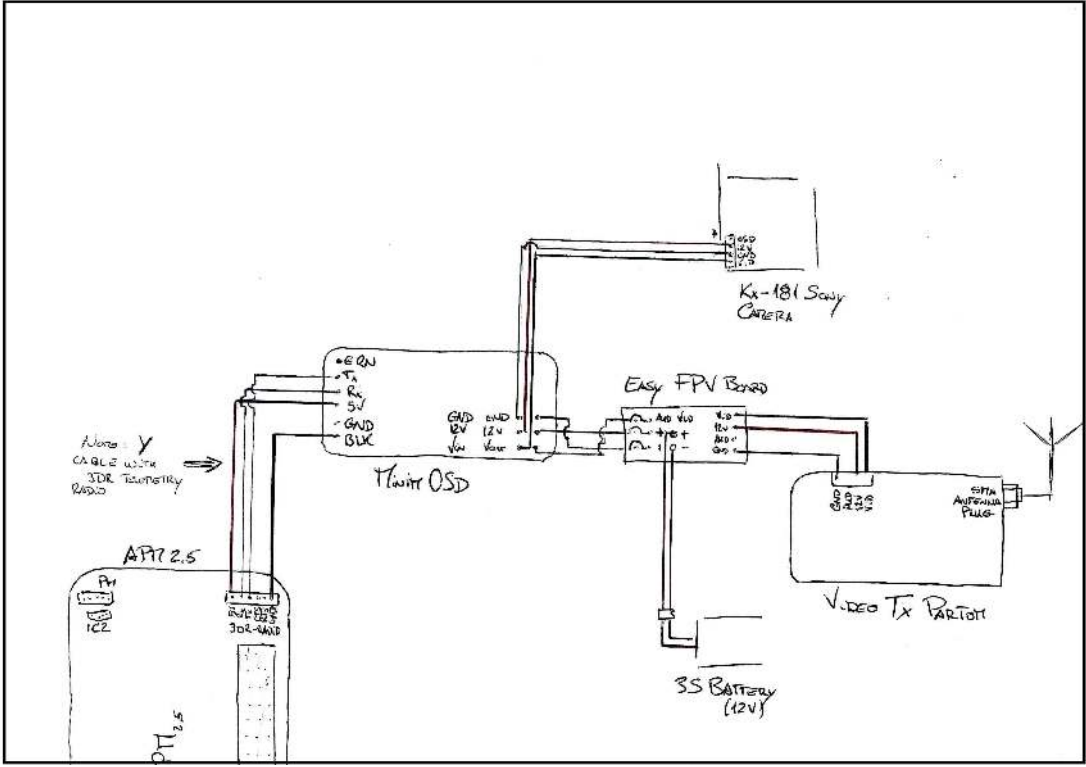
Figure C.1: Video transmission schematic.

Figure C.2: RC sub-system Schematic.